NASA
Technical
Paper
2072

September 1982

Supersonic Jet Noise Generated by Large-Scale Instabilities

John M. Seiner,
Dennis K. McLaughlin,
and C. H. Liu

NASA Technical Paper 2072

1982

Supersonic Jet Noise Generated by Large-Scale Instabilities

John M. Seiner
Langley Research Center
Hampton, Virginia

Dennis K. McLaughlin
Dynamics Technology, Inc.
Torrance, California

C. H. Liu
Langley Research Center
Hampton, Virginia

National Aeronautics and Space Administration

Scientific and Technical Information Branch

SUMMARY

The role of large-scale wavelike structures as the major mechanism for supersonic jet noise is examined. The evaluation investigates the capability of the quasi-linear instability analysis of Morris and Tam (AIAA Paper No. 77-1351 and Journal of Fluid Mechanics, May 29, 1980) to predict the evolution of large-scale flow structures and the resulting radiated noise. The evaluation compares predictions of the instability analysis with measurements of near-field sound pressures and with hot-wire or hot-film probe measurements in the flow field. These comparisons are made for unheated jets of nominal Mach numbers of 1.5, 2.0, and 2.5 for a range of Reynolds numbers from 3.7×10^3 to 5.2×10^6. The low and intermediate Reynolds number experiments were performed at Oklahoma State University, and the high Reynolds number experiments were made at the Langley Research Center. Results demonstrated that the acoustic near field contains remarkable similarities between low and high Reynolds number jets and further substantiate the importance of large-scale structures in supersonic jet noise radiation. The instability analysis predicts the peak radiation direction adequately but differs significantly from measurement in the general origin for sound emission at the higher Reynolds number. The principal region for sound emission in all flow conditions corresponds with the peak axial location of flow fluctuations. For the high Reynolds number condition, the peak region is consistent with the far-field source location measurements of Laufer, Schlinker, and Kaplan (AIAA Journal, April 1976).

INTRODUCTION

Experimental evidence obtained during the last decade indicates that some of the properties of free shear flow turbulence may be partly deterministic. In low Reynolds number, supersonic jets, the results obtained by McLaughlin, Morrison, and Troutt (refs. 1 to 5) show that the majority of noise generated is generically related to the growth and decay of organized wavelike structures. The extension of these experimental discoveries to high Reynolds number, supersonic flows is an area of current scientific interest and represents the principal focus of this paper.

From an analytical point of view, Morris and Tam (ref. 6) have managed to calculate the near noise field associated with the growth and decay of a wavelike structure in a supersonic jet. They have obtained reasonable agreement between their near-field predictions and the experimental results of Yu and Dosanjh (ref. 7) for an unheated high Reynolds number, Mach 1.5 jet. This theory, which is described more fully by Tam and Morris in reference 8, assumes that no interaction occurs between the wavelike structure and turbulent shear layer components although the mean flow field is allowed to develop as that of a fully developed turbulent mixing layer. On the basis of the good comparison obtained with the measured acoustic field of Yu and Dosanjh, their theory suggests that wave-induced stresses (ref. 9), which arise from the interaction of the wavelike and turbulent structures, may not significantly alter the growth and decay of the wavelike component. One is naturally curious then as to whether the predicted wavelike structure, which occurs as an intermediate step in their analysis, is in agreement with what one might measure in an actual flow. In addition, it is of value to determine if a similar reasonable agreement between predicted and measured near-field acoustic behavior can be obtained for a wide range of supersonic Mach and Reynolds numbers.

The significant progress offered by this theory has stimulated our interest to investigate both the local flow development and near-field acoustic behavior of supersonic jets. In this respect, detailed comparisons between this theory and measured near-field acoustic properties have been obtained for several supersonic Mach and Reynolds number conditions. In addition, phased-averaged flow measurements, obtained in earlier studies at Oklahoma State University (refs. 1 to 5) for low and moderate Reynolds numbers, are compared with theoretical predictions of the wave development. Although phased-averaged measurements have not as yet been obtained for high Reynolds number, supersonic jets, recent developments in the interpretation of wedge hot-film anemometry signals (ref. 10) have provided the additional capability to compare certain flow development features between theoretical predictions and experimental results at low Reynolds numbers.

In the context of these comparisons, the results of this paper highlight both the similarities and dissimilarities associated with the effects of Reynolds number and Mach number in supersonic jets. In this way, certain strengths and weaknesses associated with the Morris and Tam theory (refs. 6 and 8) surface in this analysis.

SYMBOLS

A_0, A_1, A_{-1} relative amplitudes of $n = 0$, 1, and -1 azimuthal modes

a_o ambient speed of sound

B wedge hot-film calibration constant

D jet exit diameter

e', E_b fluctuating and mean anemometer voltages

f frequency

k_o thermal conductivity of air at stagnation conditions

L width of probe wedge element

M Mach number

m_o $= \dfrac{d \ln \mu}{d \ln T_w}$

Nu_o Nusselt modulus

n azimuthal mode number

OAPWL overall power level, dB (re 10^{-12} W)

$Q_n(x|\omega)$ wave evolution parameter (eq. (7))

R radial microphone location from jet exit

Re jet Reynolds number, $\rho V_j D/\mu$

Re_∞ free-stream Reynolds number

r	radial distance from jet center line
$r(0.5)$	radial location where velocity equals $0.5U_c$
SPL	sound pressure level, dB (re 20 μPa)
St	Strouhal number, fD/V_j
S_u, S_ρ, S_T	anemometer sensitivity to velocity, density, and temperature, respectively
T_o	stagnation temperature
T_r, T_w	anemometer recovery and operating temperatures
U_c, U_ℓ	center-line and local velocity, respectively
u	velocity (x-component)
V_j	fully expanded jet exit velocity
x	downstream distance from nozzle
y	vertical distance from nozzle exit
α_o	anemometer temperature resistance coefficient
γ	ratio of specific heats
δ	jet shear layer thickness
η	nondimensional radial coordinate, $[r - r(0.5)]/\delta$
θ	azimuthal jet coordinate
μ	viscosity
ρ	density
τ	anemometer temperature overheat ratio, $(T_w - T_r)/T_r$
ϕ	instability wave complex phase function
ω	radian frequency
$\langle\ \rangle$	phase-averaged component of fluctuating quantity

Subscript:

o	reference quantity

A prime (') with a symbol indicates fluctuating quantity, and a tilde (~) over a symbol indicates the root mean square of a fluctuating quantity.

DESCRIPTION OF EXPERIMENTS

Facilities

The supersonic aerodynamic and acoustic measurements at low and moderate Reynolds numbers were obtained previously at Oklahoma State University with their supersonic low-pressure anechoic test chamber facility. A detailed description of this experimental apparatus and its unique capabilities has previously been reported in references 1 to 5.

The aerodynamic apparatus used at the Langley Research Center is capable of supplying dry, unheated air continuously up to 4 kg/sec. The nozzle pressure ratios can be held to within 0.3 percent of the desired set point. A computer-controlled three-axis-probe drive mechanism is available and provides a spatial accuracy of ±0.025 mm over its entire span of travel, which is less than $\pm 5 \times 10^{-4}$ jet exit diameter. Three mufflers are used to reduce upstream valve noise to less than an overall sound pressure level of 50 dB (re 20 μPa). The acoustics facility at Langley used in the present study consists of an anechoic room with working dimensions of 6.7 by 8.4 by 7.2 m. The air supply and control system is the same as that described for the aerodynamic facility, and a similar muffler system is also used in the anechoic facility.

Measurements

Of the several shock-free supersonic jet Mach numbers used in studies at Oklahoma State University, the data at Mach number 2.1 were of prime interest to the present study because of their close proximity to recently acquired aerodynamic data at Langley. These new aerodynamic data were acquired by using a shock-free flow field generated by a Mach 2.0 convergent-divergent nozzle with an exit diameter of 4.989 cm. This nozzle, as well as all other convergent-divergent nozzles listed in table I, was designed by using a method-of-characteristics approach for parallel flow at the nozzle exit. Both mean and fluctuating components were obtained along the lip line of the high Reynolds number, Mach 2.0 jet. These measurements covered the first 20 jet diameters. The mean flow measurements were obtained with supersonic pitot- and static-pressure probes. Fluctuating overall and narrow band-pass components were obtained with a wedge hot-film anemometer.

The pitot-pressure probe is a conventional square-end tube leading to an absolute pressure transducer. The accuracy of the pitot-pressure measurements was estimated to be ±0.5 percent of the full-scale reading. The pitot probe has an outside diameter of 2.2 mm with a 0.7-mm sensing port. Since this is only a small fraction of the nozzle exit diameter, excellent probe resolution was obtained in the measurements except in the shear layer near the exit region. The probe was supported by a minimum drag supersonic airfoil mounted on the three-axis-probe drive mechanism.

A number of supersonic static-pressure measurements were also made with a probe designed by Pinckey (ref. 11). These measurements were used with the pitot-pressure measurements to determine local Mach number. Along the jet lip line, static pressure was equal to ambient pressure within the uncertainty limits of the measurements. Consequently, Mach number estimates within the shear layer were normally made directly from pitot-pressure and ambient-pressure measurements. Figure 1 shows the general arrangement of the apparatus used to perform mean flow aerodynamic measurements.

The far-field acoustic measurements were performed with an array of eighteen 1/4-inch-diameter condenser microphones. The microphones were located on a fixed radius, R = 3.7 m, centered at the nozzle exit and at 7.5° intervals from 22.5° to 150° from the jet axis (downstream direction). Four contoured nozzles were used in the acoustic experiments having nominal exit Mach numbers of 1.0 (tested at M = 0.9), 1.5, 2.0, and 2.5. Near-field microphone measurements were performed for all the jets by using a traversing microphone. The range of travel of the microphone was a polar grid with R/D = 5 to 40 and angles of 15° to 90° from the jet axis. All signals were recorded on a magnetic tape recorder having a flat frequency response from dc to 80 kHz. The data were analyzed with a 1/3-octave analyzer as well as a narrow-band analyzer using an analyzing band pass of 20 Hz. Only selected results from the Mach 2.0 nozzle jet are presented in this paper in comparison with the Morris and Tam theory. Figure 2 shows the general arrangement of the mechanism used to acquire the near-field acoustic pressure data with the single microphone polar traverse.

The commercial wedge hot-film probe used in this study is shown in profile in figure 3. The probe body consists of three compound wedge angles whose leading-edge half-angle is 40°. A thin film of nickel is sputtered on each side of the leading-edge wedge section. A thin layer of quartz is coated over the nickel film to protect it from free-stream contaminants. The leading-edge section itself is composed of a quartz sublayer which leads gradually to a ceramic base in the downstream wedge sections. The probe is operated in the constant-temperature mode with a 50-Ω symmetrical bridge and with a film temperature overheat ratio τ of 0.98.

Although there is a large body of data concerning the calibration and use of hot-wire probes in low-density supersonic flows (for example, refs. 12 to 16), there has been very little use of hot-film probes in supersonic flow, particularly of the wedge geometry. The work of Glaznev (ref. 17) was the only published research found that made use of this type probe in supersonic flow. In preliminary investigations with this probe, the interpretation of its response to the fluctuating variables of density, velocity, and temperature was assumed to be similar to that for hot-wire probes. Subsequent investigations however revealed that this was not true. The wedge probe was found to have a different sensitivity to velocity fluctuations than to density fluctuations throughout the entire Mach number range, $0.5 < M < 2.0$, whereas in the range $M > 1.3$ the sensitivity of hot-wire probes to these variables is the same. Some of these new findings on wedge probe interpretation were recently reported by Seiner and Yu in reference 10.

These new results have made it possible to investigate the fluctuating flow structure of high Reynolds number, supersonic jets with a frequency response appropriate to the research requirements. The relationship between measured bridge voltage fluctuations and the fluid variable fluctuations is still interpreted with Kovasnay's method of local linearization as

$$\frac{e'}{E_b} = S_u \frac{u'}{U_\ell} + S_\rho \frac{\rho'}{\rho} - S_T \frac{T_o'}{T_o} \tag{1}$$

but it can be shown that the sensitivity ratio S_u/S_ρ, which is unity for hot-wire probes above $M = 1.3$, is given by

$$\frac{S_u}{S_\rho} = 1 + m_o(\gamma - 1)M^2 \tag{2}$$

for wedge probes. In equation (2), m_o can be taken as a constant equal to 0.765 for air between reference temperatures of 270 K to 350 K. At high free-stream Mach numbers, equation (2) indicates that the wedge probe will have a stronger dependence on velocity than on density. Measurements by Seiner and Yu (ref. 10) further show that, from the solution of equation (1), velocity also dominates the temperature component with unheated supersonic jets. Although full solution to equation (1) requires operation of the probe at a minimum of six temperature overheat ratios, the above results show that measured bridge voltage fluctuations with high film probe temperatures and free-stream Mach numbers will primarily vary with velocity fluctuations. In the present investigation, both conditions are met, and the voltage fluctuation data presented can be interpreted as a reasonable estimate for longitudinal velocity fluctuations. Thus, in this experimental range, one can approximate the velocity fluctuations as

$$\frac{u'}{U_\ell} \approx \frac{1}{S_u}\frac{e'}{E_b} \tag{3}$$

where the velocity sensitivity, as derived from the calibration data of figure 4, provides

$$S_u = 0.25\left[1 + m_o(\gamma - 1)M^2\right]\left(1 - \frac{B}{Nu_o}\right) \tag{4}$$

In equation (4), the data intercept B from figure 4 gives $B = 15.3$, and the Nusselt modulus Nu_o is computed from bridge voltage measurements through the relation

$$Nu_o = \frac{\alpha_o E_b^2}{2k_o L}\frac{\tau + 1}{\tau}\frac{R_r}{\left[R_r(\tau + 1) + R_L + 50\right]^2} \tag{5}$$

where R_r is probe recovery resistance and R_L is probe lead resistance.

The wedge hot-film results in this paper have employed equations (2) through (5) for interpretation of the probe response. The probe was mounted in a low drag supersonic wing which is shown in figure 5. The probe was positioned at points in the flow by the same digital traversing device as used in the pitot studies.

DESCRIPTION OF ANALYSIS

The calculations reported herein and compared with experimental results were performed by using the computer code LSNOIS, whose algorithms were published by Tester, Morris, Lau, and Tanna in reference 18. This computer code was based upon the quasi-linear instability analysis of Morris and Tam (ref. 6) for axisymmetric jets and Tam and Morris (ref. 8) for the plane supersonic shear layer.

For this analysis, a small disturbance of arbitrary amplitude and spectral content is presumed to exist at the nozzle exit, perhaps initiated by acoustic feedback to the nozzle exit. Once initiated these disturbances are convected downstream, where in response to changes in the mean flow, they grow rapidly near the nozzle exit and gradually decay as the mean flow diverges. The starting point for the analysis of Morris and Tam begins with the linearized inviscid equations of motion for a small disturbance in a compressible fluid medium. The analysis investigates the spatial stability of the basic mean flow through spectral decomposition of the disturbance field variables. The basic flow, which at the present time represents an empirical input in the computer program, is permitted to slowly diverge like that of a real jet flow. The mean flow divergence represents a very special feature in their analysis because, as they point out, no sound emission would be expected from a subsonically convecting disturbance in a parallel flow. The method of multiple scales is used to accommodate the wave to the mean flow divergence, and a uniformly valid matched asymptotic expansion is constructed with the far field to enable computation of the associated acoustic field.

The input and output parameters of the computerized version of this analysis are given as follows. For any specific mean jet flow condition, the analysis calculates the evolution, phase, and wave-number spectrum for specified frequency and azimuthal mode number constituents in the jet. The initial component disturbance amplitude for each frequency and mode number is the single free parameter in the calculation and, of course, is selected to provide reasonable agreement with experiment. The disturbance frequencies are selected to bracket the peak in the noise radiation spectrum in the direction of maximum noise emission. In terms of the Strouhal number, this range of disturbance frequencies varies from 0.1 to 0.5.

The jet conditions for which both flow instability and sound radiation predictions were made are tabulated in table I. Low, moderate, and high Reynolds number jet data for several jet exit supersonic Mach numbers were used in order to test this analysis with as wide a range of data as practical. In this sense, the analysis of Morris and Tam would serve as a basis for comparisons between physical observations involving this set of data.

The LSNOIS code has been developed to handle conventional high Reynolds number ($Re > 10^6$) axisymmetric supersonic jets. This code has incorporated the relevant mean flow properties obtained by Birch and Eggers (ref. 19) and Warren (ref. 20) to serve as input for the instability calculations. However, since the mean flow properties differ considerably between high and low Reynolds number jets, it was necessary to modify this code with parameterized mean flow properties associated with the data for low and moderate Reynolds number jets. To remain entirely consistent, even the high Reynolds number jets of this study were incorporated in this new portion of the code. In this way, the analysis of Morris and Tam was extended to study the effect of jet Reynolds number.

EXPERIMENTAL RESULTS

General Acoustic Features of High and Low Reynolds Number Jets

Several acoustic similarities exist between low and high Reynolds number, supersonic jets; this provided a strong stimulus for the present investigation. These similarities can be observed in the spectrum, overall power, and directivity of the radiated noise.

For the low Reynolds number jets in table I (i.e., $Re < 10^4$), the flow emerges from the nozzle exit essentially laminar, undergoes a large-scale wavelike motion in the near-field region from the jet exit, and eventually disintegrates into a random-type motion at some downstream region of the flow. The hot-wire measurements of Morrison (ref. 3) in the near-field region of the low Reynolds number, Mach 2.1 jet show that the flow field is dominated by a single frequency component at a Strouhal number St of 0.22. The corresponding acoustic spectrum, shown in figure 6(a), is composed primarily of a single frequency at the same flow Strouhal number. As the Reynolds number increases, the flow becomes increasingly random and the acoustic spectrum widens but remains centered near the same Strouhal number. Figure 6(b) shows the intermediate Reynolds number results of Troutt (ref. 5) for the Mach 2.1 jet at $Re = 7.0 \times 10^4$; figure 6(c), the high Reynolds number results ($Re = 5.2 \times 10^6$).

The spectral shapes associated with the various Reynolds number flows of figure 6 show that spectral similarity in the acoustic field is achieved with a Reynolds number as low as 7.0×10^4. Since the nature of the transition between the acoustic spectra for low and intermediate Reynolds numbers is unknown, no special significance can be attached to the Reynolds number of 7.0×10^4.

In addition to the peak Strouhal number scaling of figure 6, the data of figure 7 show that, for a wide range of supersonic jet velocities, the low Reynolds number jets radiate noise of comparable power to the conventional high Reynolds number jets. These data refer to the acoustic power radiated in the jet arc and are normalized to standard ISA conditions as recommended by the SAE in reference 21. As a final example of the similarity between the acoustic field of low and high Reynolds number jets, figure 8 shows that the overall level and directivity of the radiated noise are comparable in the dominant noise emission direction. The directivity data use the nozzle exit as a point of reference, and the data were obtained at $R/D = 40$.

The acoustic similarities that do exist between the low and high Reynolds number jet flows suggest that the dominant noise-generating mechanisms are similar. If this is true, then it is not unreasonable to apply the same type of instability analysis and noise radiation calculation to the different Reynolds number jet flows. Before doing this, it is necessary to acquire mean flow properties for a given jet flow condition since in the instability analysis the mean flow is considered as a known coefficient. In this way, at a given axial point of development downstream of the nozzle exit, the governing equations are linear to provide an analogous wave-type solution.

Mean Flow Measurements

Extensive flow-field measurements for the high Reynolds number, supersonic jets were performed only on the Mach 2.0 jet. This Mach number was chosen as a compromise between the more practical lower Mach number supersonic jets and the desire to main-

tain local hot-film probe, free-stream Mach numbers beyond unity to satisfy equation (3).

Figure 9 presents a plot of the jet center-line Mach number as a function of the downstream coordinate x. The data for both the high and intermediate Reynolds number, Mach 2.0 jets are shown in this figure. The end of the potential core (i.e., the point where the mean center-line velocity begins to decay) occurs between 8 and 9 jet diameters in the intermediate Reynolds number jet. The high Reynolds number jet shows that the potential core extends beyond the range of the intermediate Reynolds number jet to the range between 11 and 12 jet diameters. Both Reynolds number jets exhibit a similar rate of decay beyond the potential core region.

Mean velocity information (in parametric form) is provided as an optional input to the instability calculation (refs. 6 and 8). The velocity data of the high Reynolds number jet are curve fit to a half-Gaussian of the form:

$$\frac{u(\eta)}{U_c} = \begin{cases} \exp\left[-2.773(\eta + 0.5)^2\right] & (\eta > -0.5) \\ 1 & (\eta < -0.5) \end{cases} \tag{6}$$

where $\eta = [r - r(0.5)]/\delta$, U_c is the velocity on the center line of the jet at the given x location, $r(0.5)$ is the radial location where the velocity equals $0.5U_c$, and δ is the local shear layer thickness. In the initial mixing layer region $\delta = r(0.1) - r(0.9)$, which represents the radial distance between the points where the local velocity is 0.1 and 0.9 of the center-line velocity. Downstream of the end of the potential core $\delta = 2r(0.5)$ and η reduces to $\eta = (r/\delta) - 0.5$ where δ is now 1/2 the local jet diameter. (The jet diameter is the diameter of the locus of points where the mean velocity is 0.01 times the local center-line velocity at the nozzle exit.) Figure 10 shows the measured mean velocities deduced from the pitot measurements in the high Reynolds number, Mach 2.0 jet. Figure 10(a) shows the results for the first 11 jet diameters; this covers the extent of the initial mixing region. Figure 10(b) shows the results beyond this region and up to the end of the supersonic core region near 22 jet diameters. To convert from Mach number to velocity, the conventional assumption of uniform stagnation temperature is made (the jet supply and room ambient stagnation temperatures were within ±2°C for all tests).

In general, the results of figure 10 demonstrate an adequate correspondence between the measured mean profiles and half-Gaussian curve fit of equation (6). The local shear layer thickness δ and the parameter $r(0.5)$ used to generate the best curve fits are plotted in figure 11 as a function of the axial coordinate, with figure 11(c) being for the high Reynolds number jet. Comparison with the equations for the parameters given in appendix B of reference 6 shows that the measured mean flow data are almost identical to parameterized data that Morris and Tam have extracted from Birch and Eggers (ref. 19). These mean flow data, in parametric form, are incorporated in the LSNOIS computer code (ref. 18).

The development of the mean flow of supersonic jets at low Reynolds number is considerably different from conventional high Reynolds number jets. Shown in figures 11(b) and 11(a) are the mean flow parameters corresponding to the best half-Gaussian curve fits for intermediate and low Reynolds number jets, respectively. These data, extracted from Morrison (ref. 3) and Troutt (ref. 5), were obtained in

the supersonic low-pressure anechoic test chamber facility at Oklahoma State University. It is apparent that for the low Reynolds number (7.9×10^3) jet, the jet shear layer remains laminar and grows slowly for several jet diameters. Initial stages of transition to a turbulent shear layer are accompanied by a substantial growth in the shear layer finally resulting in the termination of the potential core. The intermediate Reynolds number (7.0×10^4) jet behaves much more like the high Reynolds number (5.2×10^6) jet. However, even in this jet, the first several jet diameters are required for transition to occur to a turbulent shear layer. The differences in the mean flow profiles between the low, intermediate, and high Reynolds number jets will have an effect on the results of the instability calculation.

Instability Evolution Comparisons

Aside from computing the near-field acoustic radiation generated by the instability wave model, the LSNOIS code outputs the axial evolution of the instability wave as an intermediate step in the analysis. It is important to recognize however that the computer code does not predict the wave evolution in terms of the physical variables such as velocity, density, or temperature. Instead Morris and Tam (ref. 22) characterize the wave amplitude evolution for any particular wave-number component of the spectrum with the axial variation of the quantity,

$$Q_n(x|\omega) = \frac{\exp[i\phi(x)]}{\left(M^2\omega^2 - \alpha^2\right)^{n/2}} \tag{7}$$

where $\alpha = d\phi(x)/dx$ and n is the azimuthal mode number. This quantity is the important parameter in determining the far-field directivity pattern and is used in this paper for comparison with the measured spatial variation of the flow variables.

The hot-wire data obtained in the Oklahoma State University facility are reduced in terms of fluctuations in the mass velocity ρu. The Langley data for the high Reynolds number jet are reduced in terms of longitudinal velocity fluctuations as given by equations (2) to (5). For all measurements reported in this paper, the probe was located in the middle of the shear layer (on the nozzle lip line), which is near the location of maximum fluctuating anemometer voltage. The data are normalized by dividing the root-mean-square velocity or mass velocity fluctuation by an upstream value near the exit plane. Normally a value downstream of the exit plane (for example, at 1 or 2 jet diameters) is used since the experimental uncertainty of downstream data is considerably less than measurements in the very thin shear layer near the jet exit. A similar procedure is used to normalize the magnitude of $Q_n(x|\omega)$ in equation (7).

Low Reynolds Number, Supersonic Jets

The instability analysis should work best when applied to the low Reynolds number jets since in these jets the shear layer is laminar for a major portion of the jet development. In this laminar region consideration of a Reynolds stress model is unimportant. Figure 12 presents the axial distribution of normalized mass velocity fluctuations in the low Reynolds number (7.9×10^3), Mach 2.1 jet. This normalization is accomplished by referencing the value obtained for these data at a specified axial location. The open symbols represent measurements of the full spectrum of mass

velocity fluctuations. However, the major portion of the energy is concentrated in a narrow band around a frequency St of 0.22. The curve represents the results of the LSNOIS predictions for the St = 0.22 frequency component with the mean flow specified in figure 11(a) as the input to the code. The calculation was performed for the n = 1 helical mode since Morrison (ref. 3) established that this is the predominant mode of the instability. Again it is emphasized that there is only one specified constant in this calculation. In this flow, the matching was performed at x/D = 2 as shown by the solid square symbol in figure 12.

Morrison (ref. 3) was also able to determine the evolution of the coherent portion of the mass velocity fluctuations by measuring the phase-averaged portion of the hot-wire signal. In Morrison's study, a jet excitation signal, a glow discharge, is used to time the phase-averaged measurement. He has shown that the excitation is relatively weak and has a small influence on the development of both the instability and the mean flow. The results of the phase-averaged measurements are plotted as solid circular symbols in figure 12 and are in reasonable agreement with the prediction for the growth portion of the curve and in the axial location of maximum fluctuations. However, the overall gain is underpredicted by approximately 25 percent.

Comparisons between experiment and prediction were also made for the low Reynolds number, Mach 1.4 and Mach 2.5 jets. (See figs. 13 and 14.) For each one, the mean flow parameters, which were provided as input to the instability analysis, were extracted from Morrison (ref. 3). The symbols in figure 13 represent the same quantities as those in figure 12. The open symbols represent the full spectrum of normalized mass velocity fluctuations (the energy is concentrated around St = 0.33), the solid circular symbols are the phase-averaged (coherent) portion of the measurements, and the solid square represents the point at which the prediction is matched to the experiment. As in the M = 2.1 data, the axial location of the peak flow fluctuation is in agreement with the peak wave amplitude location as expressed by the quantity $Q_n(x|\omega)$. The growth rate prediction is initially within experimental uncertainty of the data, but the overall gain is underpredicted.

The comparison in figure 14 between experiment and prediction in the Mach 2.5 jet shows that the analysis overpredicts the overall gain by 30 percent. In this figure phase-averaged data are not included. However, for this jet the percentage of coherent fluctuations is 90 percent for the first 16 jet diameters so that the coherent wave evolution would be only slightly below the existing data. Although there is a discrepancy between prediction and experiment in overall gain the predicted wave evolution has a similar shape and location of the peak amplitude level.

In summary, the instability analysis predicts a wave evolution similar to what is observed in the peak flow fluctuation levels for all three low Reynolds number, supersonic jets. This is shown by the similarity in the initial growth rates and axial locations of the peak values. Both the data and predicted wave behavior peak at increasing downstream locations with increasing jet Mach numbers. This trend is consistent with the observed increased length of the potential core region with increasing jet Mach number. In the present Morris and Tam analysis, the decay rate of supersonically traveling waves is not rigorously calculated; this represents one area which requires further development. However, the results of comparison between predictions and Morrison's experimental results (ref. 3) do not indicate that the approximate calculation of the decaying supersonic waves is any further from experimental results than is the rigorous calculation of decaying subsonic waves for the M = 1.4 jet.

Moderate Reynolds Number, Mach 2.1 Jet

Before presenting the results of prediction for the moderate Reynolds number jet it is appropriate to summarize the experimental results of Troutt (ref. 5). He established that the moderate Reynolds number ($Re = 7.0 \times 10^4$) jet developed much more like a high Reynolds number jet than like a low Reynolds number jet. This is demonstrated by the mean flow properties shown in figure 15. In the naturally excited jet, the flow fluctuations possess relatively broad spectra with peaks that shift to lower and lower frequencies with downstream position. Near the jet exit, measurements indicated that the natural excitation is very broad in spectral content, whereas the low Reynolds number jets have a naturally occurring discrete frequency instability. When the low Reynolds number jets are artificially excited with a pure tone at the naturally occurring dominant frequency, there is little change in the development of the instability or the mean flow. In the moderate Reynolds number jet, there is a dramatic change in the spectral distribution of the flow fluctuations as the energy concentrates near the single frequency of excitation. Since the mean flow development is not changed drastically, Troutt argues that wave properties such as wavelength and phase velocity are probably similar in the excited and unexcited jets.

Figure 15 presents the results of hot-wire measurements made in the $Re = 7.0 \times 10^4$, Mach 2.1 jet with the probe located in the middle of the shear layer approximately on the nozzle lip line. The narrow-band data at a Strouhal number St of 0.19 are shown in figure 15(a); the data at $St = 0.38$, in figure 15(b). These frequencies were chosen to bracket the relatively broad peak in the spectrum of noise radiated in the maximum noise emission direction of the jet (as previously shown in fig. 6(b)). Two prediction curves are drawn corresponding to the $n = 0$ mode (axisymmetric mode), shown as the dashed line, and the $n = 1$ helical mode. The data of figure 15 show a resemblance to the initial predicted wave growth and axial location for peak amplitude. Beyond this peak amplitude region, the data indicate a slower rate of decay for each Strouhal number component than that predicted for the wave decay. However in the band-pass data of figure 15, fluctuations which are not coherent with the upstream wave system are included in the measurement, whereas only the coherent portion is represented by the instability theory.

Troutt (ref. 5) has performed phase measurements in both the flow field and in the near acoustic field. These measurements have shown that the discrete waves in the jet can be described by a combination of the $n = 0$, $+1$, and -1 modes. (There is no difference between the predicted wave properties of the $n = +1$ and -1 helical modes.) By assuming a wave composed of the axisymmetric, right- and left-hand helical modes according to

$$\frac{\langle \rho u \rangle}{\rho u} = A_0 + A_1 e^{i\theta} + A_{-1} e^{-i\theta}$$

Troutt was able to estimate from phase-averaged measurements the relative amplitude level between the modes at the jet exit and several downstream locations. He found that, for $St = 0.19$, A_0/A_1 equals 1.4 and, for $St = 0.38$, A_0/A_1 equals 0.5. Thus, the axisymmetric mode dominates the lower frequency wave, and the helical mode dominates the higher frequency component.

The phased-averaged (coherent) portion of the hot-wire signal in the moderate Reynolds number, Mach 2.1 jet is shown in figure 16. These phase-averaged data are in better agreement with the predicted wave evolution than are the results at St = 0.19 in figure 14. In this case, the predicted wave evolution is obtained through a linear combination of the n = 0, +1, and -1 modes in the proportion $A_0/A_1 = 1.4$ as suggested by the measurements of Troutt. The solid square symbol again indicates the point at which both the predicted wave evolution and experiment are matched.

Troutt has shown that excitation of the jet with the point glow discharge device has an influence on the jet fluctuations as well as a measurable influence on the mean flow development. The spatially averaged jet flow developed slightly faster in terms of downstream distance than did the unexcited jet. The parameters δ and r(0.5) corresponding to the excited and natural jets presented in figure 17 demonstrate the effect of this excitation. The distribution of mean flow parameters shown by the dotted line corresponds to the excited jet case. This mean flow condition was provided as input into the instability calculation of the wave evolution shown in figure 16. In view of the approximate method of apportioning the content of the n = 0, +1, and -1 modes and the application of spatially averaged mean flow profiles from a slightly asymmetric situation, the agreement between experiment and predicted wave behavior in figure 16 is very encouraging.

High Reynolds Number, Mach 2.0 Jet

In the experiments for the low and moderate Reynolds number jets, the coherent portion of the wave was determined by phase averaging the hot-wire signal with the excitation signal for timing. In the present high Reynolds number experiments, no excitation mechanism had been devised; therefore, a phase-averaged measurement was not possible.

The results of the wedge hot-film measurements are presented in figure 18. As for the low and moderate Reynolds number jets, the probe was located in the middle of the shear layer (at r/D = 0.5). Shown in figure 18(a) are the narrow-band data at St = 0.2 and in figure 18(b), the data at St = 0.4. These frequencies correspond approximately to the frequencies used for the moderate Reynolds number jet (fig. 15). Also, the LSNOIS instability predictions are presented by a dashed line for the n = 0 mode and a solid line for the n = 1 mode. As previously noted, the narrow-band data at moderate jet Reynolds number, the decay portion predicted for the wave amplitude behavior in the high Reynolds number flow, significantly differ from the measured axial variations of relative longitudinal turbulence intensity levels. There is also a large difference in the axial location of the peak amplitude level. The relative peak amplitude levels between measured data and the instability prediction are satisfactory for St = 0.2 with only the n = 1 mode and may be reasonable for St = 0.4 with a suitable combination of the n = 0, +1, and -1 modes. It is reasonable to assume, based on the moderate Reynolds number results of figure 16, that phased-averaged measurements in the high Reynolds number jet would appear more representative of the wave amplitude predicted evolution.

Since little prior experience exists with the wedge hot-film probe, a test of the probe frequency response was made by examining the similarity of measured spectra in the shear layer. First, consider spectra obtained by the probe located on the jet lip line between x/D = 2.25 and 10, as shown in figure 19(a). The power spectra are presented in terms of Strouhal number based on the exit diameter and velocity. The amplitude of the spectra are shown at the power spectrum level and have been nor-

malized by the jet exit velocity. The trends existing in the spectra suggest that spectral similarity for the supersonic mixing layer could be obtained by assuming that frequency scales linearly with local mean velocity and inversely with increasing downstream distance. In figure 19(b), the same five power spectra are compared on the basis of this local Strouhal number. The amplitude levels were adjusted to equivalent spectrum levels through multiplication by $\frac{U_\ell}{V_j}\frac{D}{x}$. The spectral similarity for the supersonic mixing layer demonstrated that the wedge hot-film probe had sufficient high frequency response for the current experiments.

As a final point of discussion on the hot-film measurements for the high Reynolds number jet, the hot-film amplitude distributions of figure 18 show a similar peak amplitude location as that of the broadband noise source distribution measured by Laufer, Schlinker, and Kaplan (ref. 23). They used a directional microphone system located at various positions in the far field from which estimates were made of the axial distribution of noise source strength in several supersonic jets. The comparison demonstrates the similarity in shape and in the axial location of peak amplitude between the hot-film measurements in the jet and the directional microphone measurements focusing on the jet.

Near-Field Measurements and Comparison With Prediction

As mentioned earlier, Morris and Tam (ref. 6) have compared their near-field predictions with measurements performed by Yu and Dosanjh (ref. 7) with a Mach 1.5 perfectly expanded cold jet. Morris and Tam showed that, for frequencies St of 0.125, 0.25, and 0.50, the predicted near fields were in reasonable agreement with the experimental results. Our comparisons were conducted primarily on Mach 2.0 jets, for which, as previously discussed, the predicted instability evolutions are in reasonable agreement with the phase-averaged portion of the flow fluctuation.

Figure 20 presents the near-field experimental and predicted sound pressure level contours for the low Reynolds number, Mach 2.1 jet measured by Morrison (ref. 3). An elementary estimation for the direction and origin of sound emission in this figure is indicated by an arrow and its axial intercept. The calculations were performed for the $n = 1$ mode at $St = 0.22$, which corresponds to the measured dominant instability as shown by figure 6(a). The absolute level of the calculations has been adjusted at only one point. The predictions demonstrate the predominant downstream emission as evidenced by the lobed shape of the sound pressure level contours. The predicted and measured sound fields appear to emanate from a region 10 diameters downstream, which corresponds to the peak flow fluctuation region shown in figure 12. However the predicted directivity is at a larger angle from the jet axis than the measurements indicate. Figure 21 shows a similar comparison between the analysis and the measurements of Troutt (ref. 5) on the moderate Reynolds number, Mach 2.1 jet for a frequency of $St = 0.19$. Figures 21(b) and 21(c) show the predictions corresponding to the $n = 0, +1$, and -1 modes. Troutt established that the near field primarily consists of these modes. There appear to be no important differences between the $n = 0$ and $n = 1$ predictions. Since this is also true in other jet calculations, only the predominant $n = 1$ data will henceforth be shown. The tracing through the sound pressure level lobes indicates the region of dominant noise generation to be further downstream in the experimental data as compared with the predicted data. These measured SPL contours are more consistent with peak amplitude location in the narrow-band hot-wire data of figure 18(a). A similar

result is apparent in the acoustic data of the high Reynolds number, Mach 2.0 jet shown later.

Figure 22 presents the comparison between measured and predicted near-field data for the moderate Reynolds number, Mach 2.1 jet for St = 0.38. The comparison demonstrates that the predicted noise field appears similar in contour pattern to the measured sound field. Although the peak emission location is the same between prediction and measurement, the predicted contours occur at a shallower angle to the jet axis for this case. The small-scale oscillations in otherwise smooth sound pressure level contours of figure 22(b) occur because of an insufficient resolution in step size in the Fourier transform of the wave amplitude evolution data. This was determined by decreasing the step size in the LSNOIS code; figure 22(b) represents a major improvement over initial results.

Figures 23 and 24 show comparisons between measured and predicted sound pressure level data for the high Reynolds number, Mach 2.0 jet. Figure 23 shows results for the St = 0.2 component; figure 24, the St = 0.4 component. These experimental data were obtained in the present study at Langley with a 1/3-octave-band analyzer. As in both the low and moderate Reynolds number jet data, these data show a general agreement between prediction and measurement in the overall contour shape. In the high Reynolds number jet, both the St = 0.2 and 0.4 components are predicted to emerge nearer the jet exit than indicated by the measured results. This same difference is seen to exist in the flow fluctuation results of figure 18. Both prediction and measured contour results indicate the same basic wave direction for each Strouhal number component.

DISCUSSION OF RESULTS

The similarity of the measured acoustic field in terms of the spectrum shape, directivity, and overall sound power radiated suggests that a similar physical mechanism governs the production of sound over a wide range of supersonic jet Reynolds numbers. The comparison in the peak radiation direction between the measured and predicted sound pressure level contours yields some promising results. The predictions show the strongly directional character of the measurements, as the general shape of the measured and predicted SPL contours are similar. Although the predicted and measured contoured acoustic data agree in angle of emission to within 10°, the axial location for predominant emission of sound is poorly predicted in the high Reynolds number jet for both the 0.2 and 0.4 Strouhal number components. The peak associated with the high Reynolds number flow fluctuation data is in much better agreement with the apparent origin for peak sound emission for both Strouhal number components. These axial locations correspond to that indicated by the broadband noise source distributions measured by Laufer, Schlinker, and Kaplan (ref. 23) for a similar high Reynolds number, Mach 2.0 jet.

The agreement between the measured and predicted peak acoustic emission locations improves as the jet Reynolds number decreases. At the lowest jet Reynolds number, the apparent origin is the same although the LNOIS code overpredicts the peak angle of emission by 10°. In general, an improved correlation can also be observed with decreasing jet Reynolds number between the axial location of the measured peak flow fluctuations and the predicted instability wave evolution. In addition, the axial locations for the peak flow fluctuations correspond well to the location for peak acoustic emission for all Reynolds and Strouhal numbers examined. Comparisons between the relative variation of the measured flow fluctuations and instability wave

evolution behavior show that the growth rate increases with decreasing Mach number (figs. 12 to 14) and increasing Reynolds number (figs. 15 and 18).

The disappointing agreement between the peak axial locations of the measured flow fluctuations and instability wave behavior in the high Reynolds number jet should be considered further. Even though a phase-averaged component was not obtained for the high Reynolds number flow, the phase-averaged measurements at the intermediate Reynolds number indicate that the axial location for peak fluctuation level would be the same since only the decay portion appears to change. It is important to recognize that the major nonlinear effect in the Morris and Tam analysis (ref. 6) is incorporated into the analysis by empirical input, namely, the accommodation of the wavelike disturbance to the mean flow variation. Although this feature is essential in the acoustic analysis, it assumes that wave-induced stresses, those that occur from turbulence-wave interactions, do not effect the growth or decay of the unstable wave. This is one area of the analysis where one might expect certain inaccuracies to occur in the computed results. However, it is not known whether this assumption leads to any greater inaccuracies than those associated with the neglect of nonlinear wave-wave interactions which are eliminated from consideration by use of the linearized perturbation equations.

To a certain extent the experimental results reported herein indicate that these nonlinear effects may be important. Since the acoustic spectra remain centered near the low Reynolds number tone, the scaling of the acoustic power in figure 7 suggests that spectral widening with Reynolds number may occur because of a spectral redistribution of energy to other scales by nonlinear interaction between flow component fluctuations. In the low Reynolds number jets, the exit flow is essentially laminar and the evolving wavelike flow structure grows slowly and is not modified by the presence of turbulence in the shear layer. For these jets, the predicted and measured peak axial location is in good agreement. With advancing jet Reynolds number, the modification to the growth of the wavelike structure due to its interaction with turbulence in the shear layer could account for the deteriorating agreement in the peak axial location. Further investigation in this area is obviously required.

CONCLUDING REMARKS

This paper reports on both aerodynamic and acoustic similarities associated with supersonic free jet shear layers. The study evaluates the evolution of flow disturbances as they grow and decay in the downstream direction and compares their near acoustic field. Aerodynamic results from three convergent-divergent nozzles with a nominal Mach number of 2 are examined to determine the effect of Reynolds number on the evolution of flow disturbances. These nozzles have Reynolds numbers of 7.9×10^3, 7.0×10^4, and 5.2×10^6 based on exit conditions. The acoustic results additionally include other Mach number jets ranging from 0.9 to 2.5 having Reynolds numbers from 3.7×10^3 to 8.84×10^6. Both the aerodynamic and acoustic results at Mach 2.0 are also compared with a theoretical prediction based on the linearized inviscid equations of motion.

The acoustic data show that the low Reynolds number jets radiate a comparable acoustic power to the high Reynolds number jets and follow the same power-law variation with jet exit velocity. In addition the acoustic data also show that for a given jet exit Mach number, the peak Strouhal number for the acoustic spectrum is independent of the jet Reynolds number.

The aerodynamic measurements are found to be in agreement with the prediction of the axial location for maximum wave amplitude for the Reynolds number jets at and below 7.0×10^4. The flow fluctuation in the high Reynolds number jet attains its peak level 7 to 8 jet diameters downstream of the predicted peak wave amplitude. The measured axial location for peak flow fluctuations is in agreement with the apparent origin for sound emission from the shear layer for all three Reynolds number conditions. Both the aerodynamic peak and apparent origin for sound emission shift downstream with increasing Reynolds numbers. The predicted acoustic results agree with the measured main acoustic beam direction for all three Reynolds number conditions.

The comparisons in this paper suggest that a similar physical mechanism exists for supersonic jet noise emission for a wide range of jet Reynolds numbers and that this mechanism is strongly dependent on the behavior of coherent type structures in the flow. The comparisons between measured results and theory, while not entirely satisfactory, represent an encouraging sign in the analysis of supersonic jet noise.

Langley Research Center
National Aeronautics and Space Administration
Hampton, VA 23665
August 19, 1982

REFERENCES

1. McLaughlin, Dennis K.; Morrison, Gerald L.; and Troutt, Timothy R.: Experiments on the Instability Waves in a Supersonic Jet and Their Acoustic Radiation. J. Fluid Mech., vol. 69, pt. 1, May 13, 1975, pp. 73-95.

2. McLaughlin, Dennis K.; Morrison, Gerald L.; and Troutt, Timothy R.: Reynolds Number Dependence on Supersonic Jet Noise. AIAA J., vol. 15, no. 4, Apr. 1977, pp. 526-532.

3. Morrison, Gerald Lee: Flow Instability and Acoustic Radiation Measurements of Low Reynolds Number Supersonic Jets. Ph. D. Thesis, Oklahoma State Univ., Dec. 1977. (Available from Univ. Microfilms as Order No. 7811060.)

4. Morrison, G. L.; and McLaughlin, D. K.: The Noise Generation by Instabilities in Low Reynolds Number Supersonic Jets. J. Sound & Vib., vol. 65, no. 2, July 22, 1979, pp. 177-191.

5. Troutt, Timothy Ray: Measurements on the Flow and Acoustic Properties of a Moderate Reynolds Number Supersonic Jet. Ph. D. Thesis, Oklahoma State Univ., July 1978. (Available from Univ. Microfilms as Order No. 7903753.)

6. Morris, P. J.; and Tam, C. K. W.: Near- and Far-Field Noise From Large-Scale Instabilities of Axisymmetric Jets. AIAA Paper No. 77-1351, Oct. 1977.

7. Yu, J. C.; and Dosanjh, D. S.: Noise Field of Coaxial Interacting Supersonic Jet Flows. AIAA Paper No. 71-152, Jan. 1971.

8. Tam, Christopher K. W.; and Morris, Philip J.: The Radiation of Sound by the Instability Waves of a Compressible Plane Turbulent Shear Layer. J. Fluid Mech., vol. 98, pt. 2, May 29, 1980, pp. 349-381.

9. Reynolds, W. C.; and Hussain, A. K. M. F.: The Mechanics of an Organized Wave in Turbulent Shear Flow. Part 3. Theoretical Models and Comparisons With Experiments. J. Fluid Mech., vol. 54, pt. 2, July 25, 1972, pp. 263-288.

10. Seiner, J. M.; and Yu, J. C.: Acoustic Near Field and Local Flow Properties Associated With Broadband Shock Noise. AIAA-81-1975, Oct. 1981.

11. Pinckney, S. Z.: A Short Static-Pressure Probe Design for Supersonic Flow. NASA TN D-7978, 1975.

12. Kovásznay, Leslie S. G.: Turbulence in Supersonic Flow. J. Aeronaut. Sci., vol. 20, no. 10, Oct. 1953, pp. 657-674, 682.

13. Morkovin, Mark V.: Fluctuations and Hot-Wire Anemometry in Compressible Flows. AGARDograph 24, Nov. 1956.

14. Rose, William C.: The Behavior of a Compressible Turbulent Boundary Layer in a Shock-Wave-Induced Adverse Pressure Gradient. NASA TN D-7092, 1973.

15. Demin, V. S.; and Zheltukhin, N. A.: Interpretation of Hot-Wire Anemometer Readings in a Flow With Velocity, Pressure, and Temperature Fluctuations. Fluid Mech. - Soviet Res., vol. 2, no. 3, May-June 1973, pp. 64-75.

16. Ko, C. L.; McLaughlin, D. K.; and Troutt, T. R.: Supersonic Hot-Wire Fluctuation Data Analysis With a Conduction End-Loss Correction. J. Phys. E: Sci. Instr., vol. 11, no. 5, May 1978, pp. 488-494.

17. Glaznev, V. M.: Some Features of the Propagation of a Discrete Tone Perturbation in a Free Supersonic Jet. Fluid Mech. - Soviet Res., vol. 2, no. 3, May-June 1973, pp. 76-79.

18. Tester, B. J.; Morris, P. J.; Lau, J. C.; and Tanna, M. K.: The Generation, Radiation and Prediction of Supersonic Jet Noise - Volume 1. AFAPL-TR-78-85, Vol. 1, U.S. Air Force, Oct. 1978. (Available from DTIC as AD A065 020.)

19. Birch, Stanley F.; and Eggers, James M.: A Critical Review of the Experimental Data for Developed Free Turbulent Shear Layers. Free Turbulent Shear Flows, Volume I - Conference Proceedings, NASA SP-321, 1972, pp. 11-40.

20. Warren, Walter R., Jr.: An Analytical and Experimental Study of Compressible Free Jets. Publ. No.: 23,885, Univ. Microfilms, Inc., 1957.

21. Gas Turbine Jet Exhaust Noise Prediction. ARP 876, Soc. Automot. Eng., Mar. 1978.

22. Morris, Philip J.; and Tam, Christopher K. W.: On the Radiation of Sound by the Instability Waves of a Compressible Axisymmetric Jet. Mechanics of Sound Generation in Flows, E.-A. Müller, ed., Springer-Verlag, 1979, pp. 55-61.

23. Laufer, J.; Schlinker, R.; and Kaplan, R. E.: Experiments on Supersonic Jet Noise. AIAA J., vol. 14, no. 4, Apr. 1976, pp. 489-497.

TABLE I.- EXPERIMENTAL JET CONDITIONS OF NOZZLES FOR COMPARISON WITH INSTABILITY AND SOUND RADIATION CALCULATIONS

Mach number, M	Reynolds number, Re	Jet diameter, D, cm	OAPWL, dB	V_j/a_o
1.4	3.7×10^3	1.00	162.2	1.19
2.1	7.9	1.00	171.4	1.53
2.5	8.7	0.90	175.8	1.67
2.1	7.0×10^4	1.00	171.6	1.53
0.9	1.0×10^6	3.96	147.8	0.84
1.5	2.5	4.28	163.6	1.24
2.0	5.2	5.00	169.1	1.49
2.5	8.8	5.08	172.3	1.67

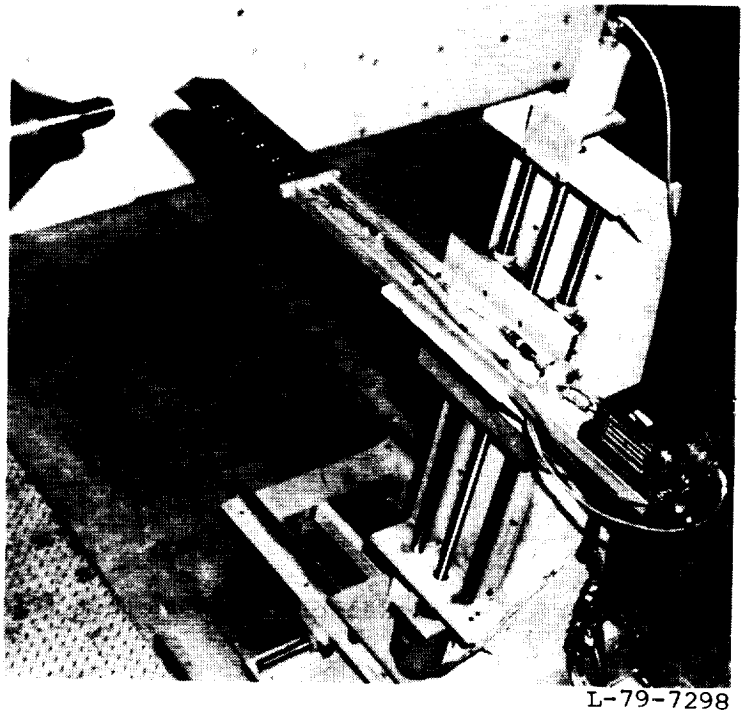

L-79-7298

Figure 1.- Apparatus used for supersonic jet noise aerodynamic measurements.

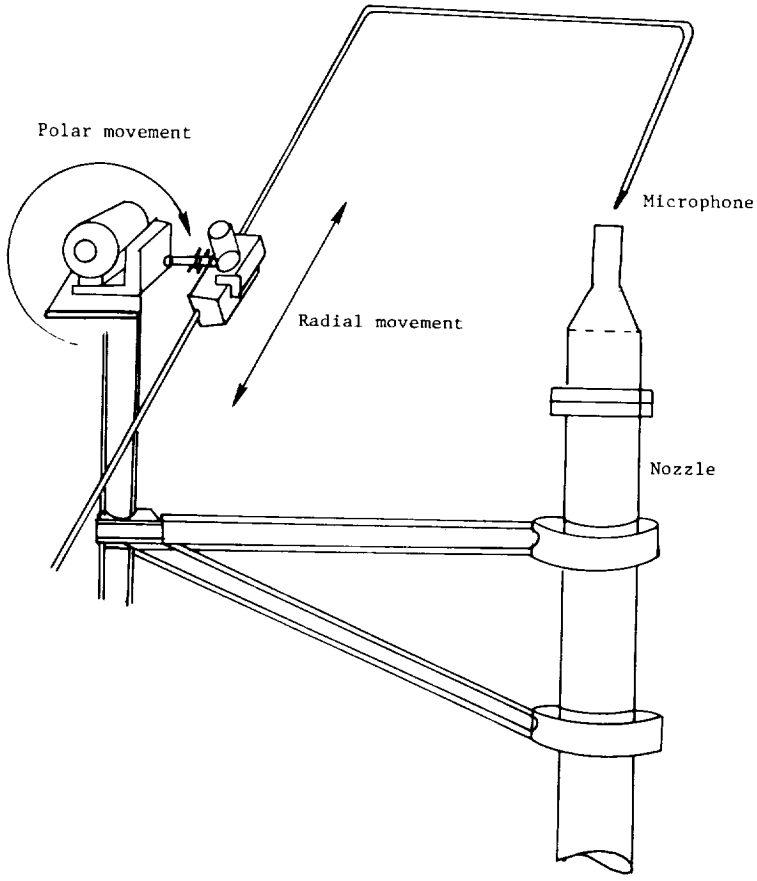

Figure 2.- Acoustic near-field polar traverse arrangement.

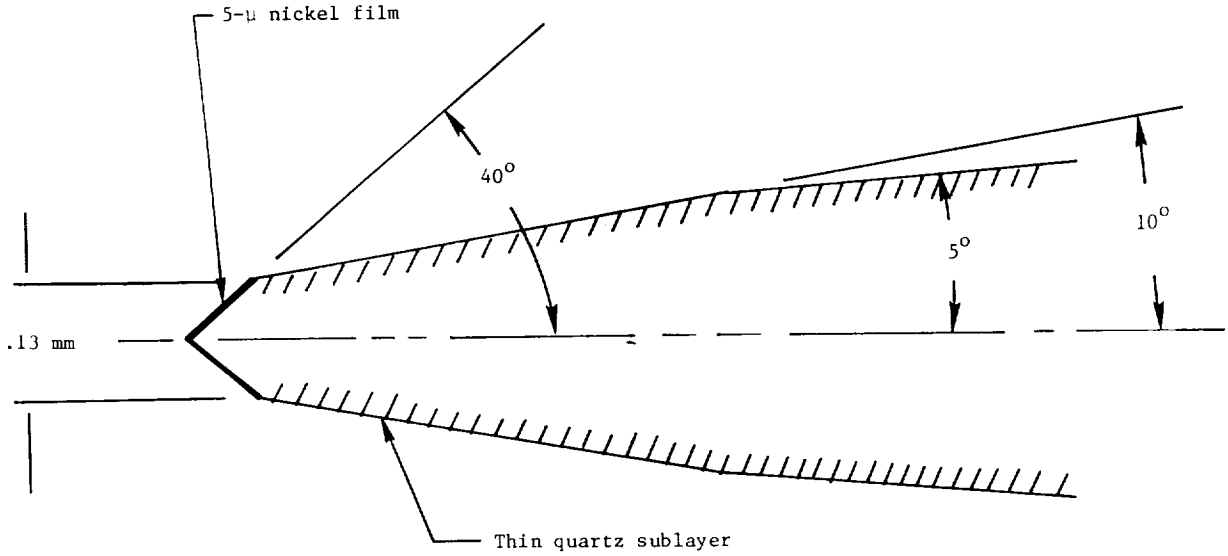

Figure 3.- Profile view of nickel-plated wedge hot-film probe.

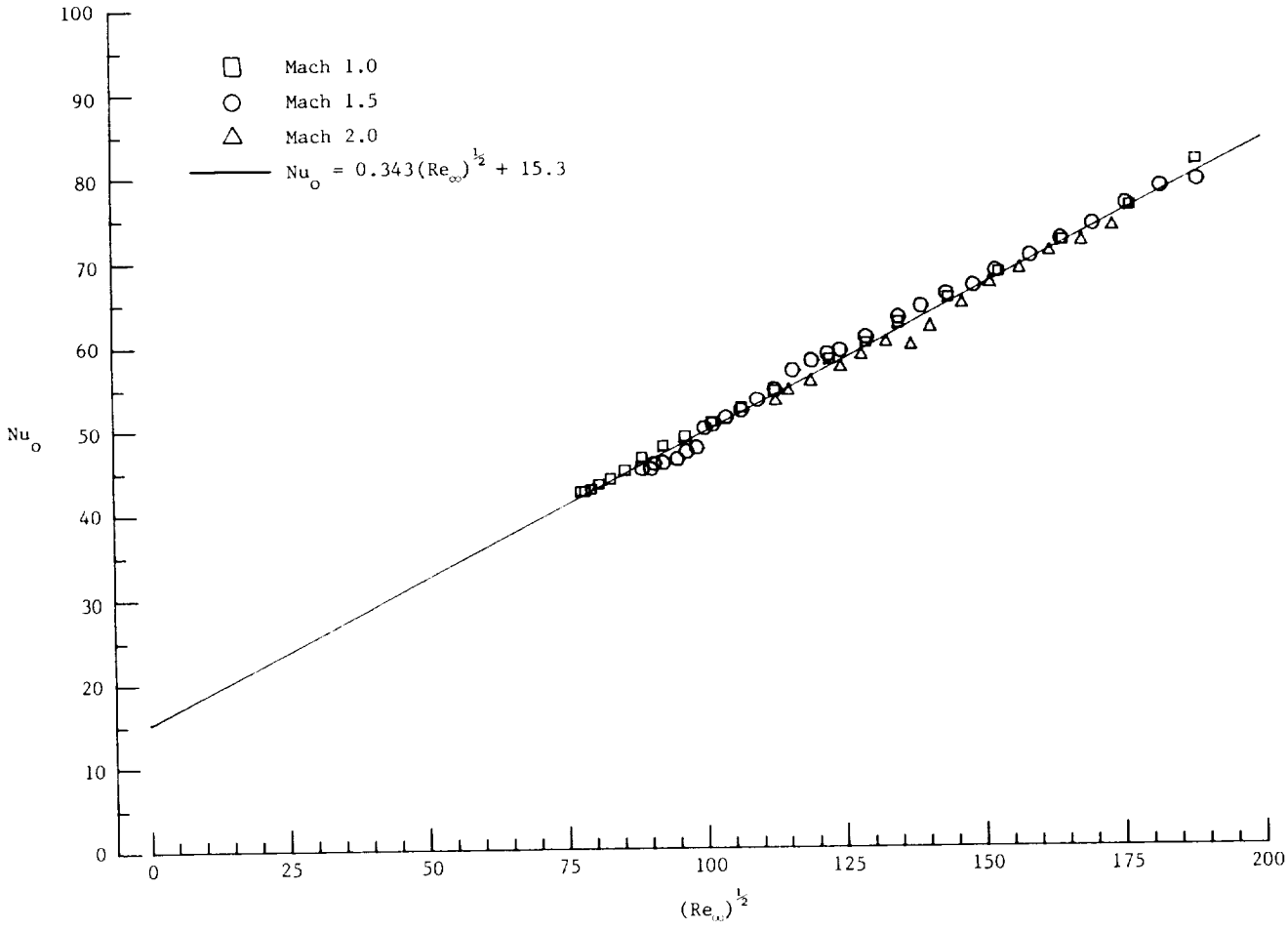

Figure 4.- Wedge hot-film calibration data.

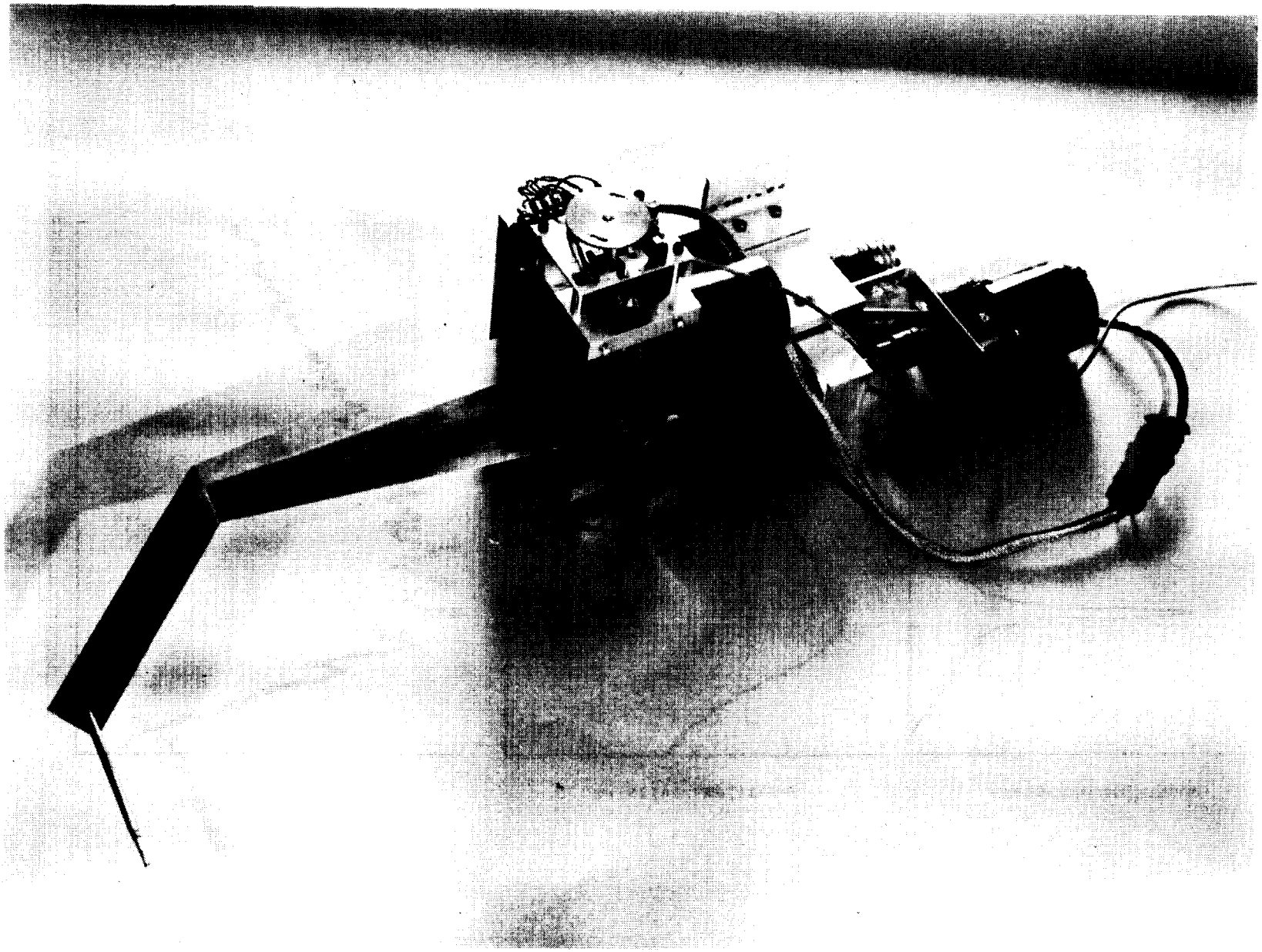

L-79-7299

Figure 5.- Hot-film supersonic wing with probe.

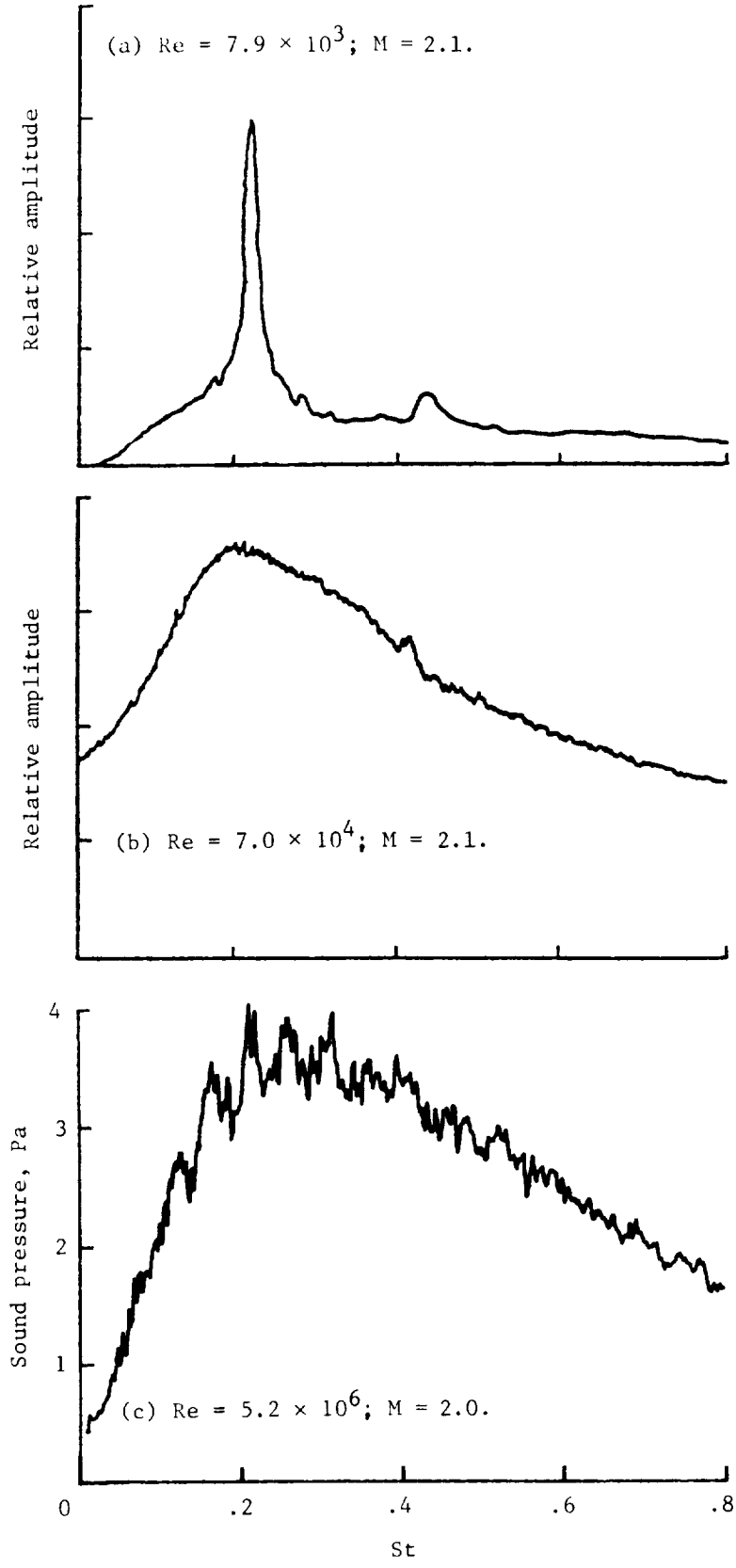

Figure 6.- Effect on acoustic spectrum with increasing Reynolds number.

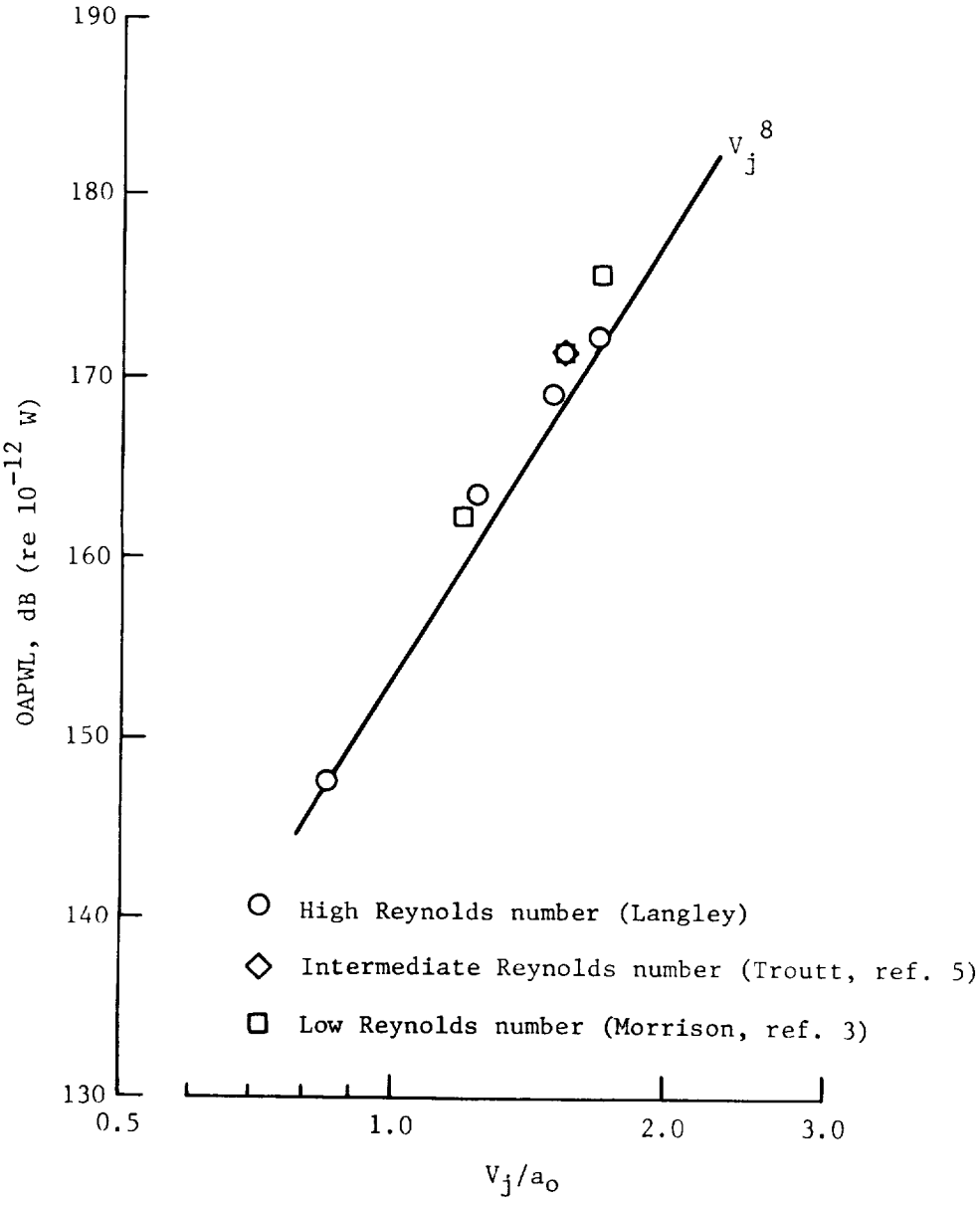

Figure 7.- Jet arc acoustic power.

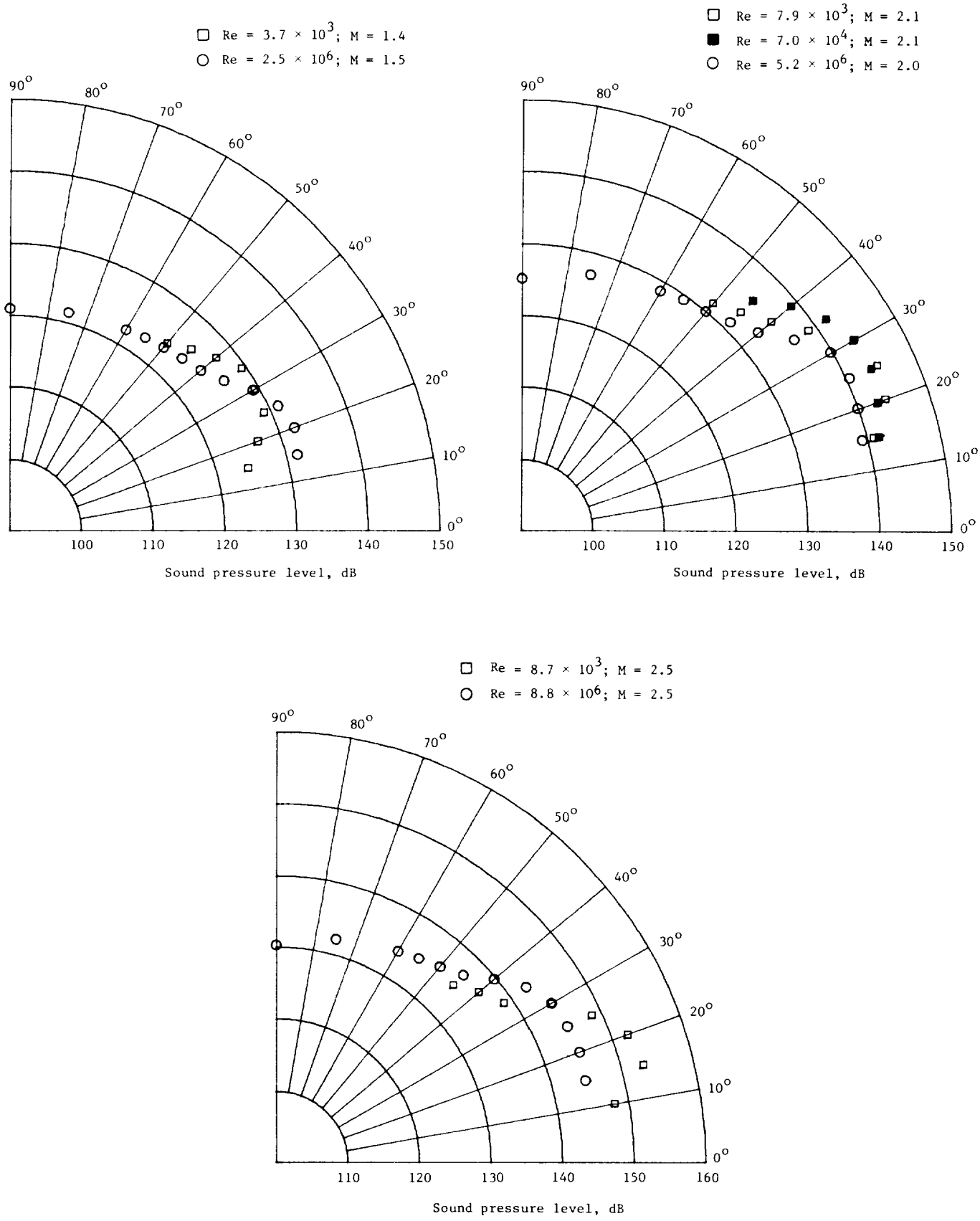

Figure 8.- Directivity of overall sound pressure level. R/D = 40.

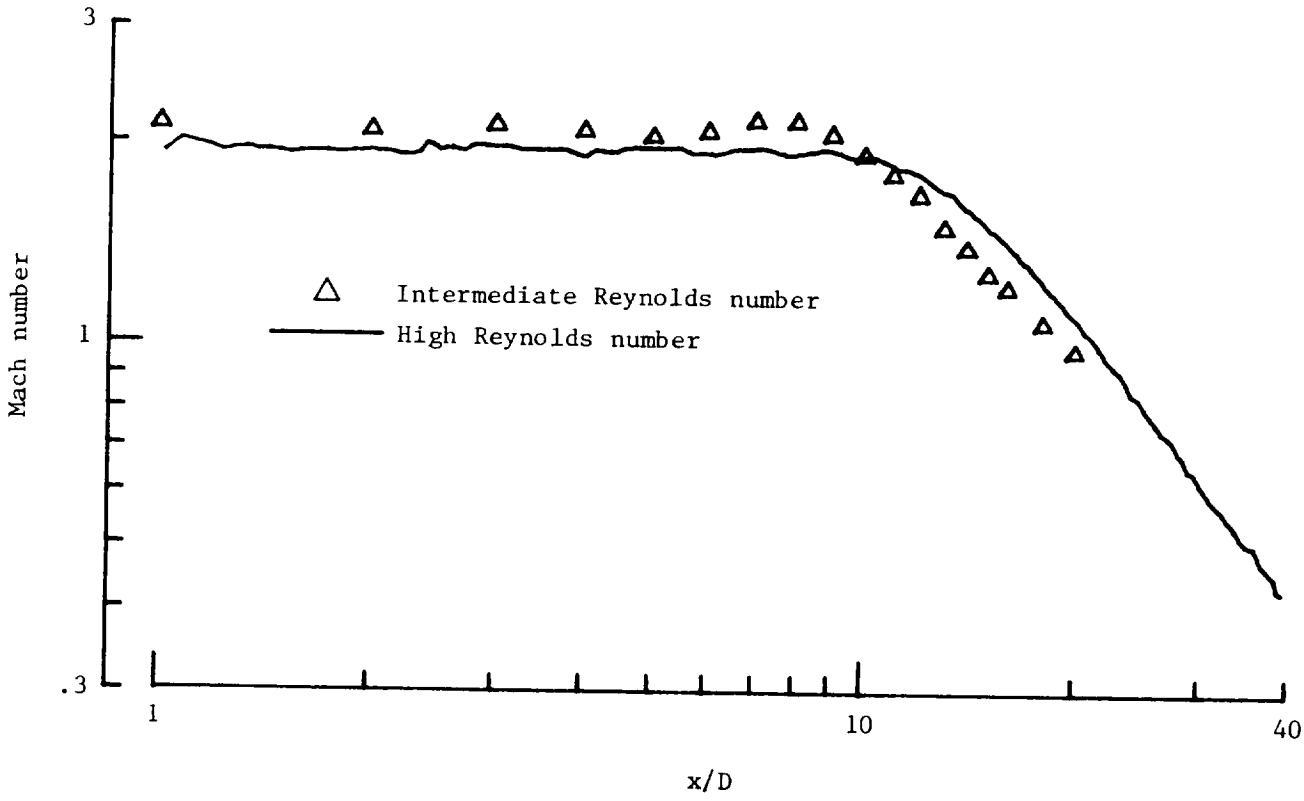

Figure 9.- Center-line Mach number distributions in Mach 2 jets.

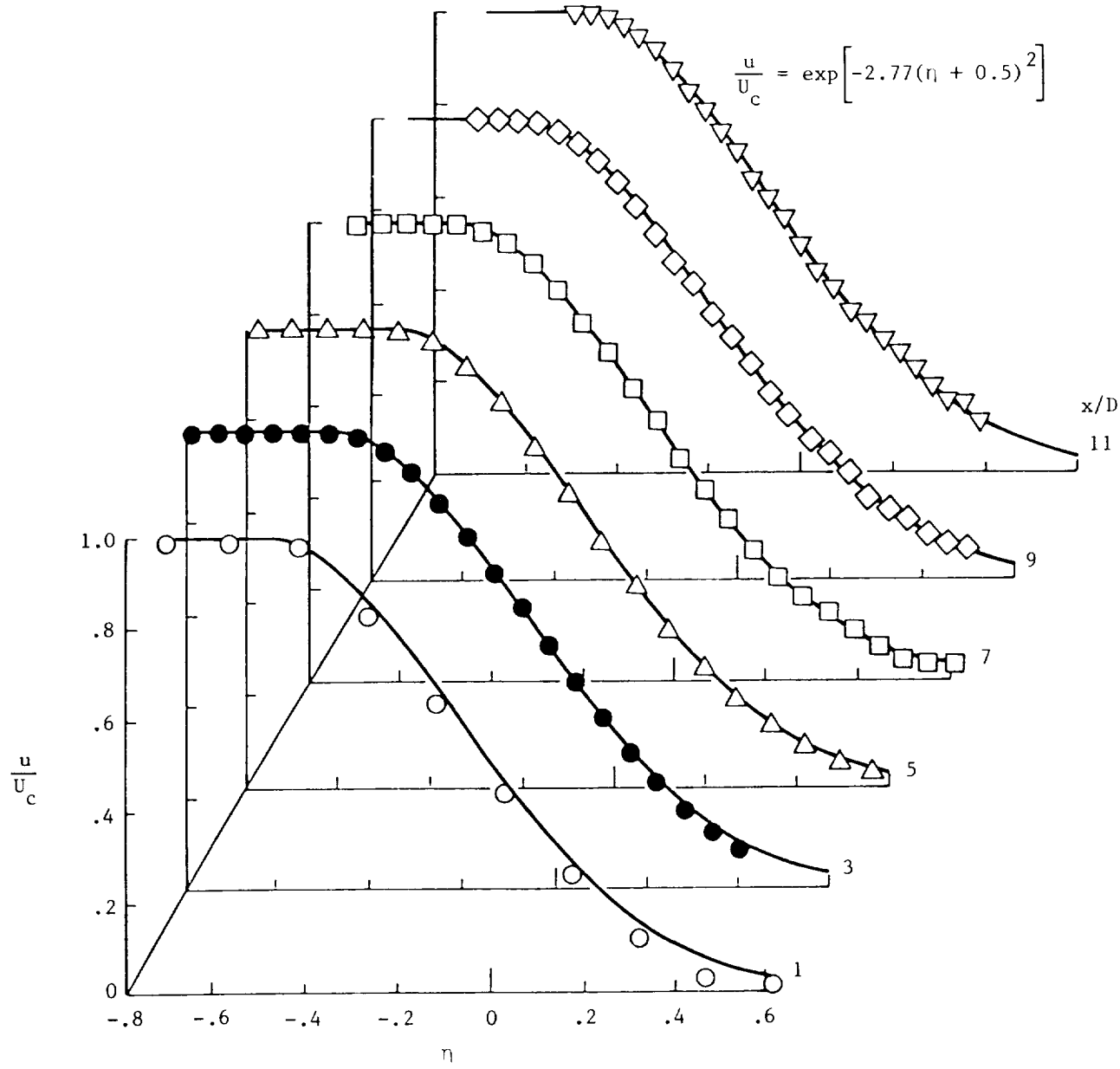

(a) x/D = 1 to 11.

Figure 10.- Mean velocity data for Re = 5.2×10^6, Mach 2.0 jet.

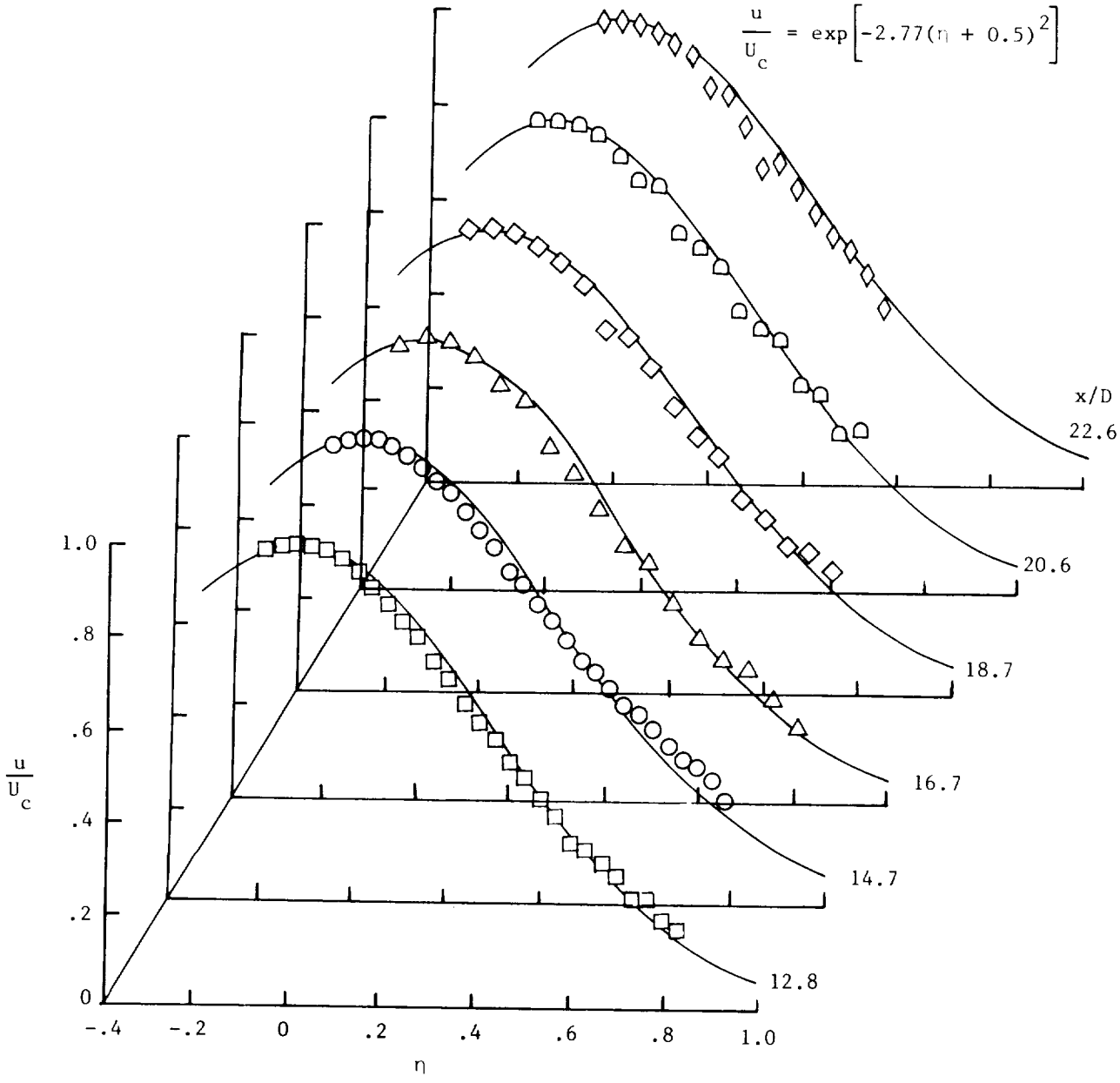

(b) x/D = 12.8 to 22.6.

Figure 10.- Concluded.

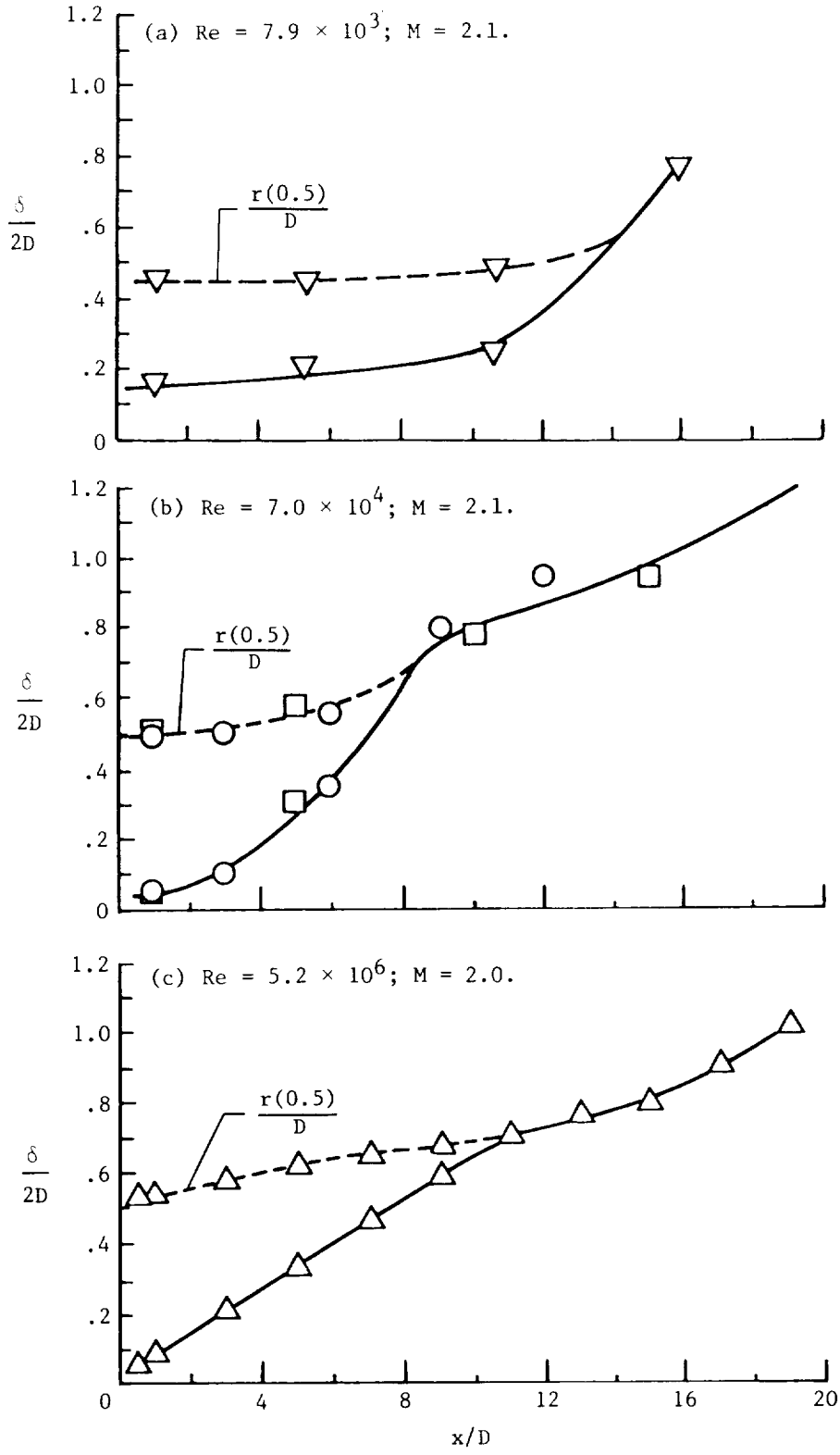

Figure 11.- Axial distribution of mean velocity parameters.

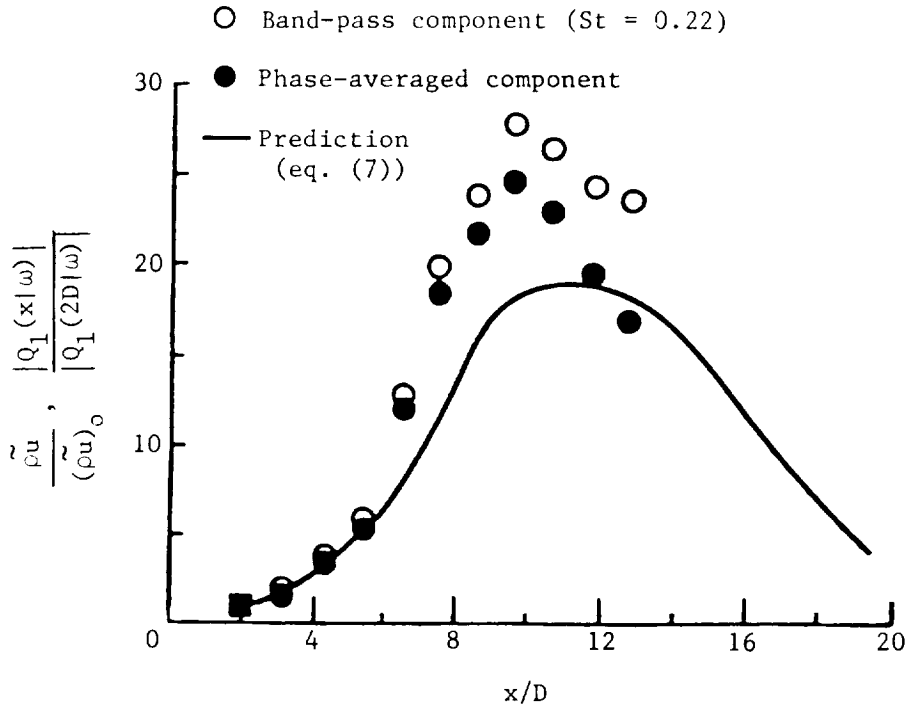

Figure 12.- Axial distribution of mass velocity fluctuation amplitude in jet shear layer for Re = 7.9×10^3, Mach 2.1 jet. r/D = 0.5.

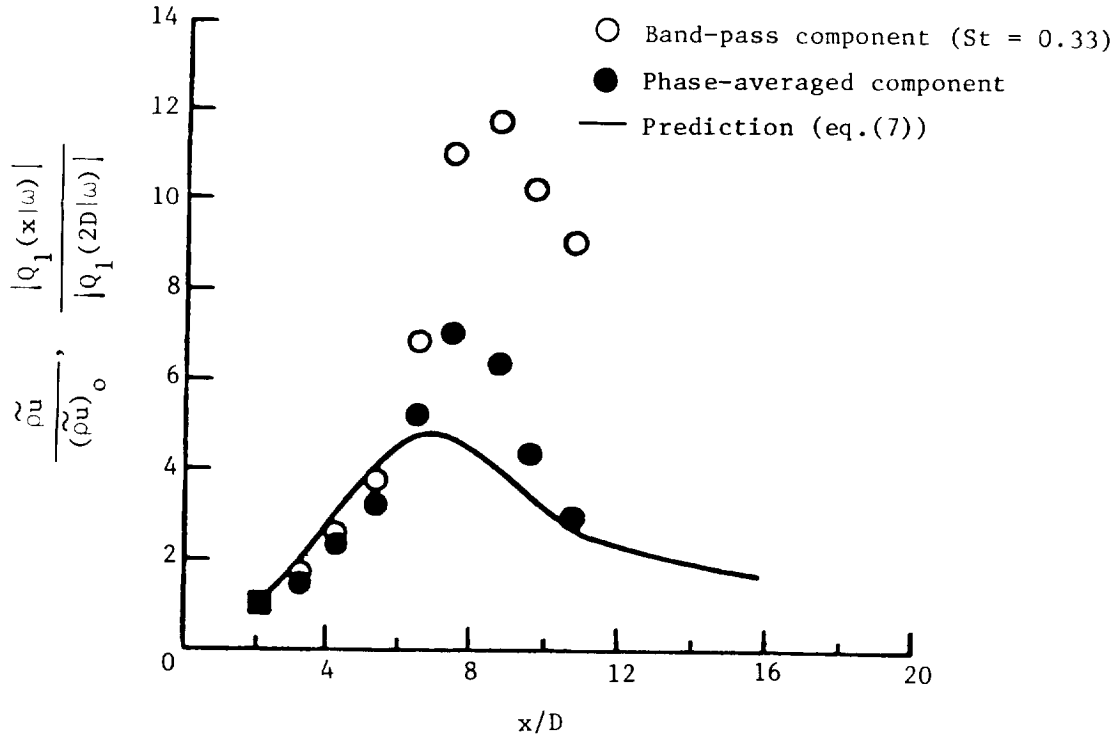

Figure 13.- Axial distribution of mass velocity fluctuation amplitude in jet shear layer for Re = 3.7×10^3, Mach 1.4 jet. r/D = 0.5.

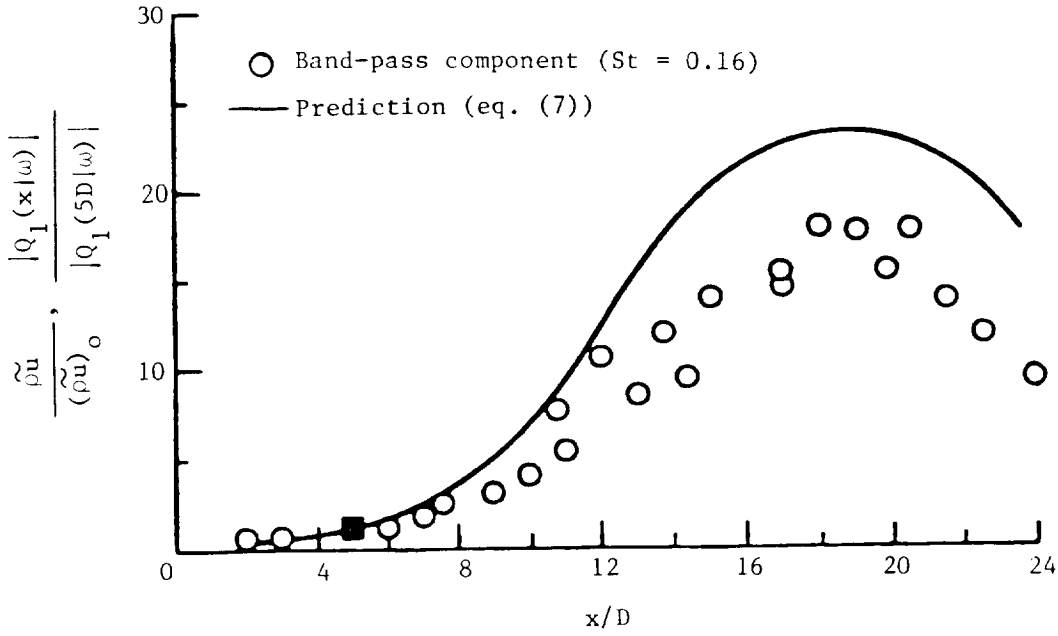

Figure 14.- Axial distribution of mass velocity fluctuation amplitude in jet shear layer for Re = 8.7×10^3, Mach 2.5 jet. r/D = 0.5.

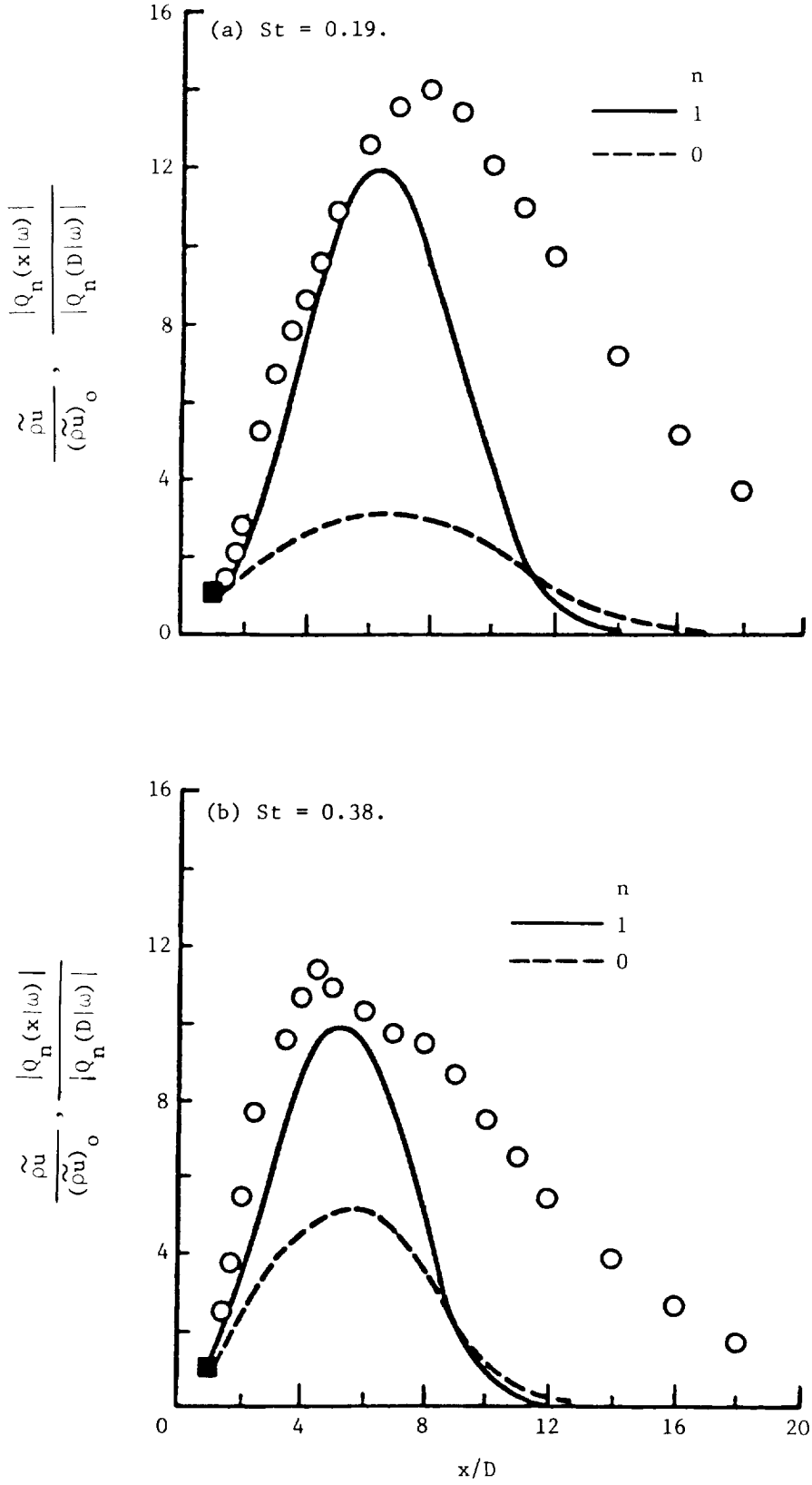

Figure 15.- Axial distribution of narrow-band mass velocity fluctuation amplitude in jet shear layer for Re = 7.0×10^4, Mach 2.1 jet. r/D = 0.5.

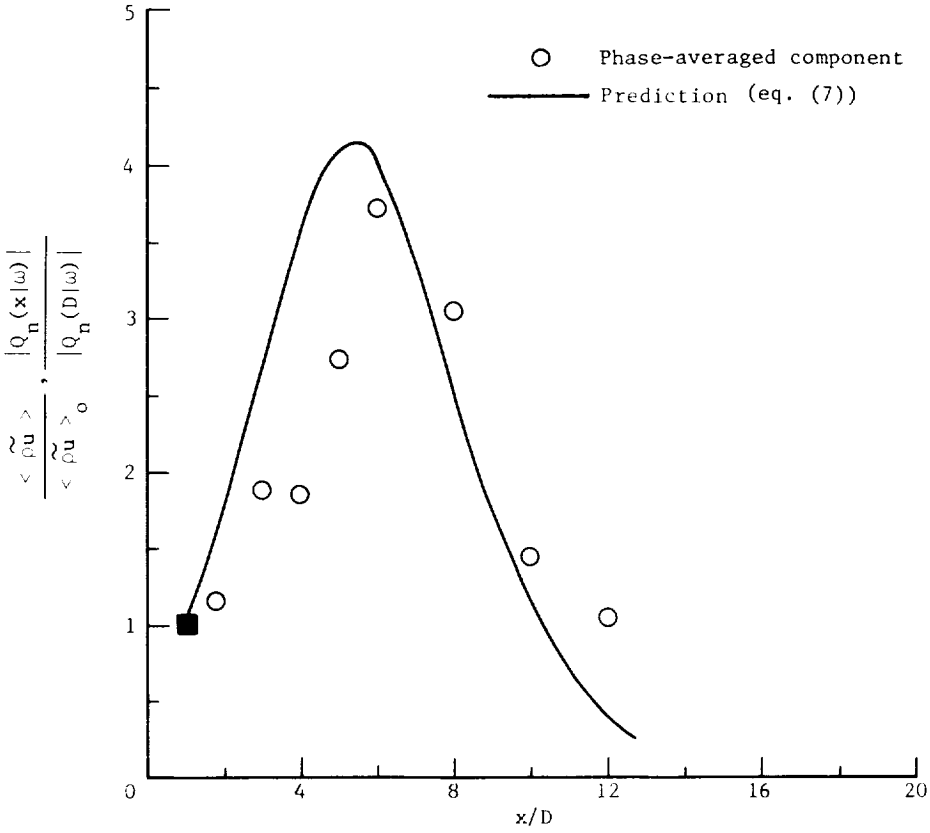

Figure 16.- Axial distribution of phase-averaged mass velocity fluctuation amplitude in jet shear layer for Re = 7.0 x 10^4, Mach 2.1 jet. St = 0.19; r/D = 0.5.

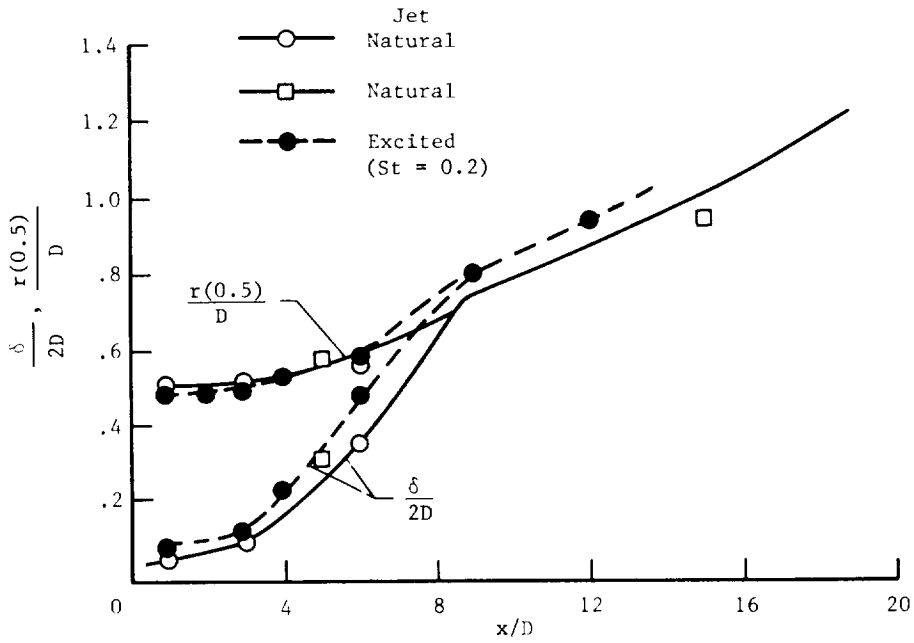

Figure 17.- Axial distribution of mean velocity profile parameters for natural and excited Re = 7.0 x 10^4, Mach 2.1 jet.

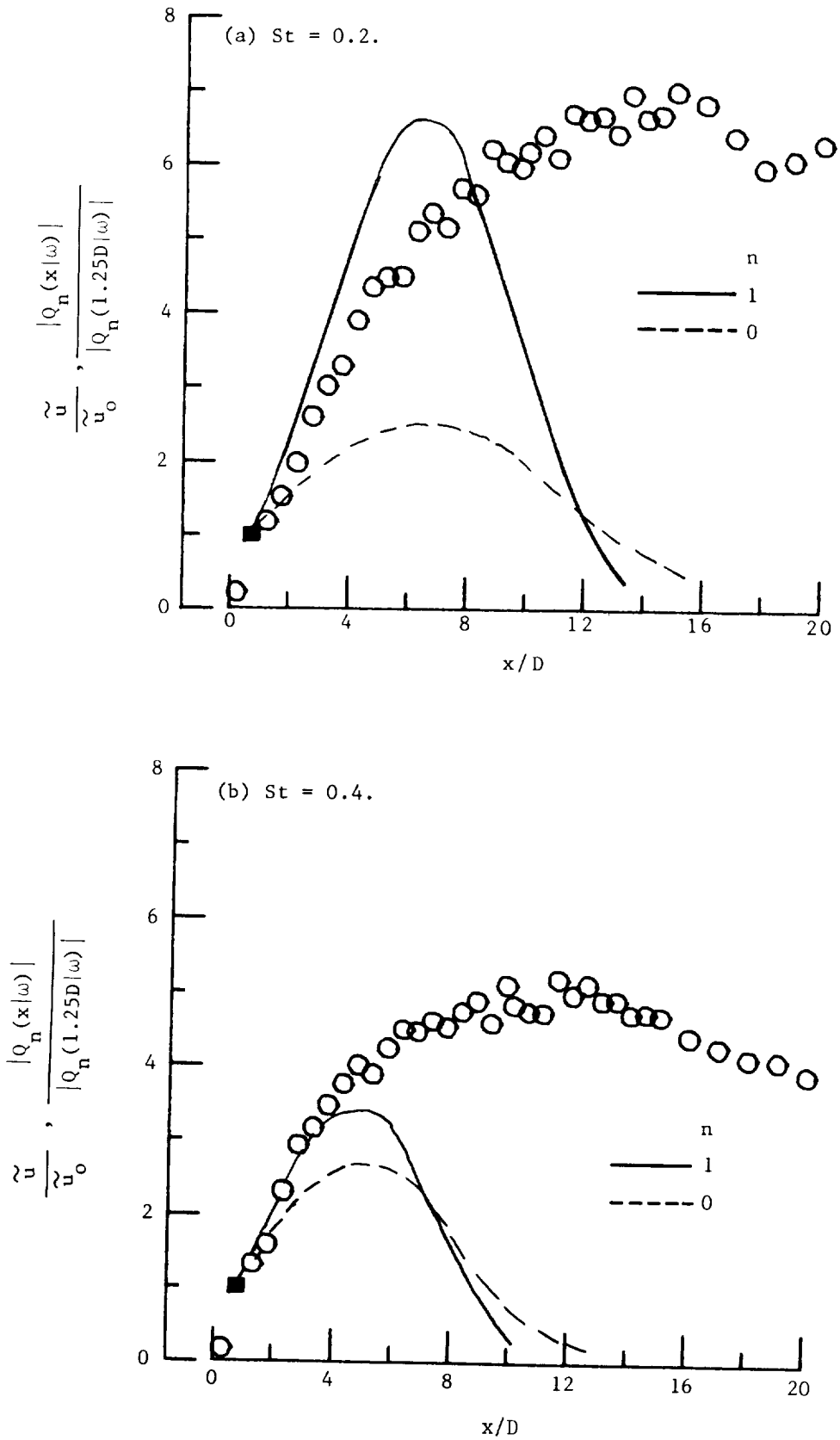

Figure 18.- Axial distribution of velocity fluctuation amplitudes in jet shear layer for Re = 5.2×10^6, Mach 2.0 jet. r/D = 0.5.

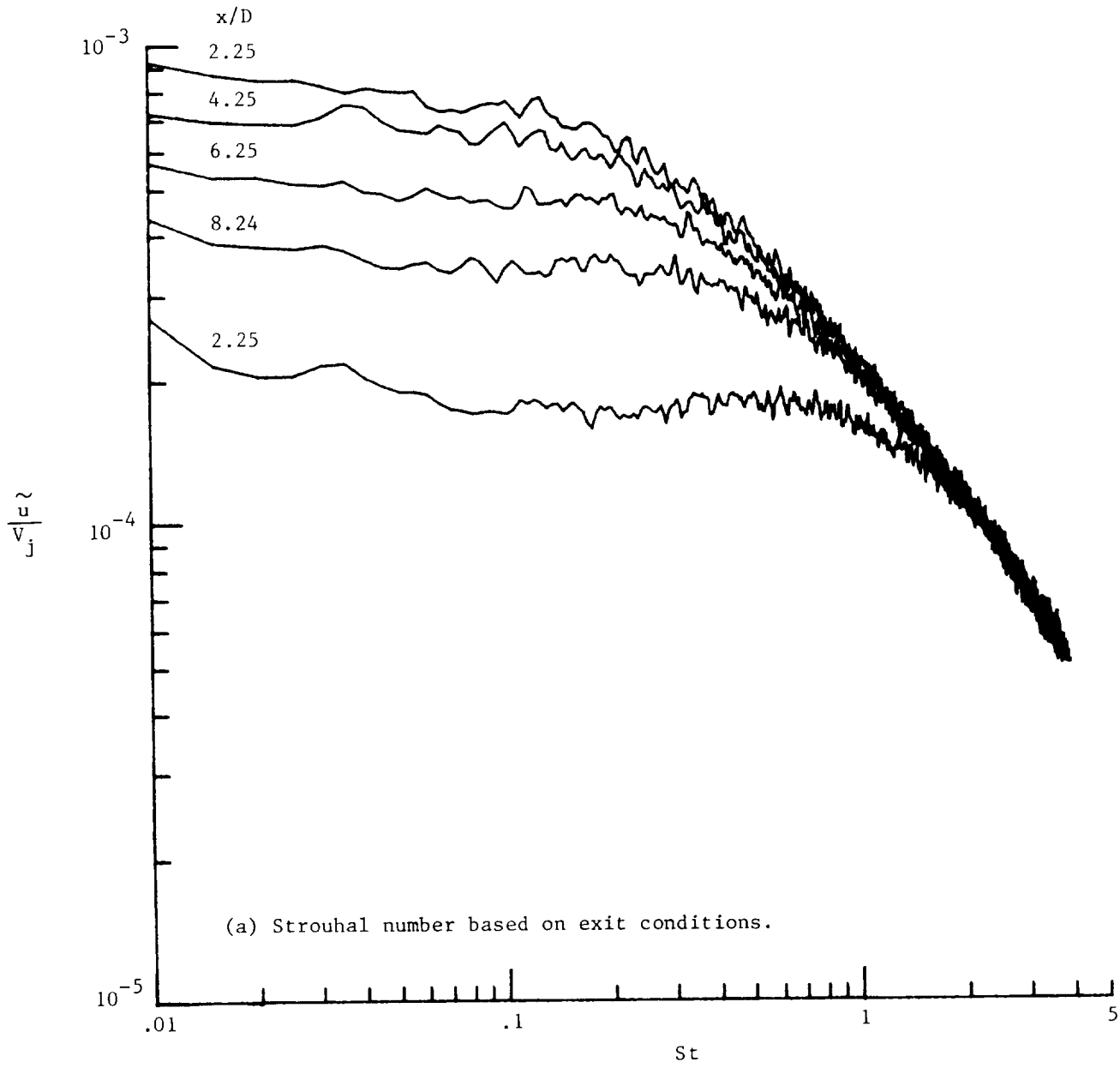

Figure 19.- Velocity spectra for high Reynolds number, Mach 2.0 jet.

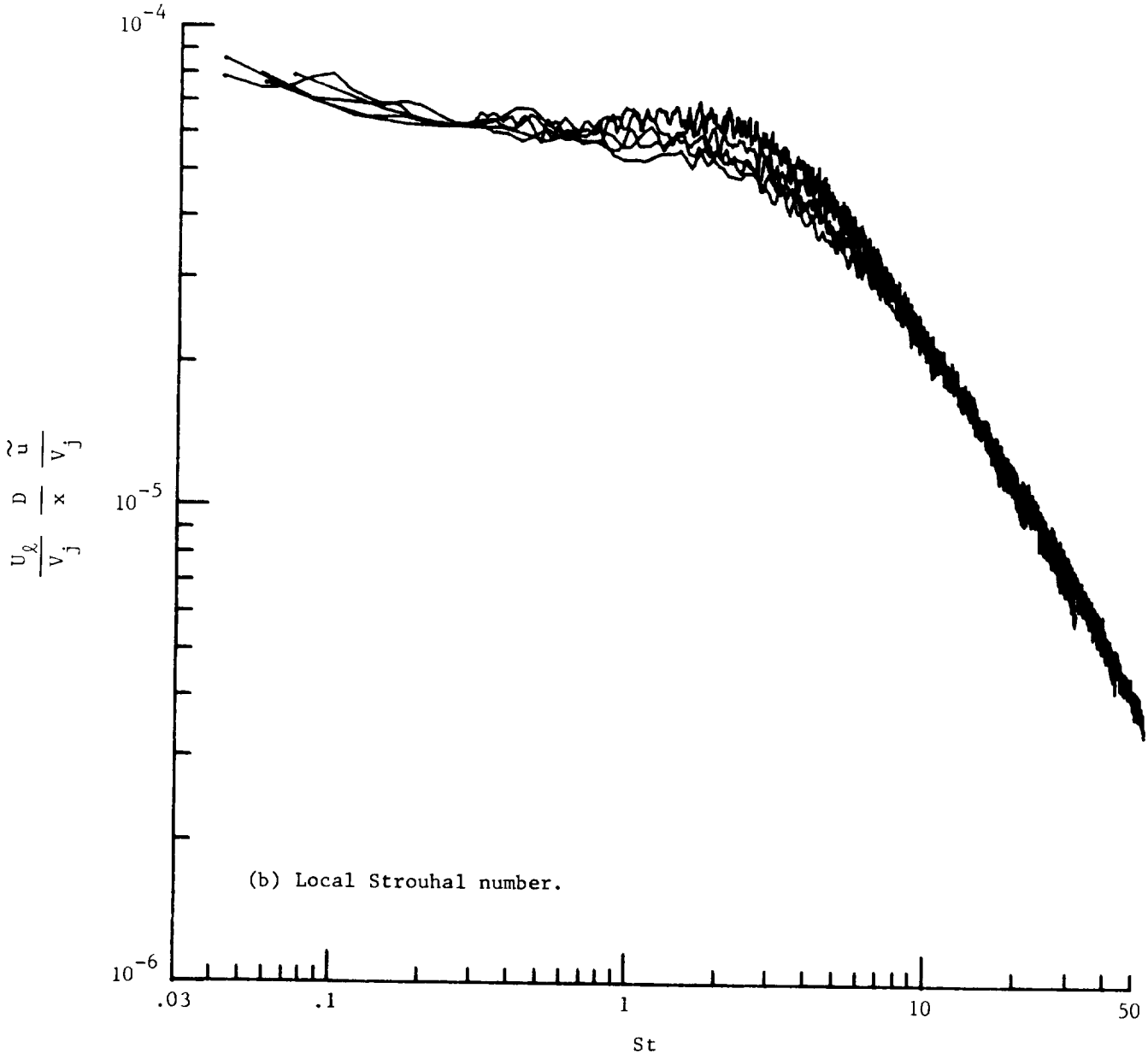

Figure 19.- Concluded.

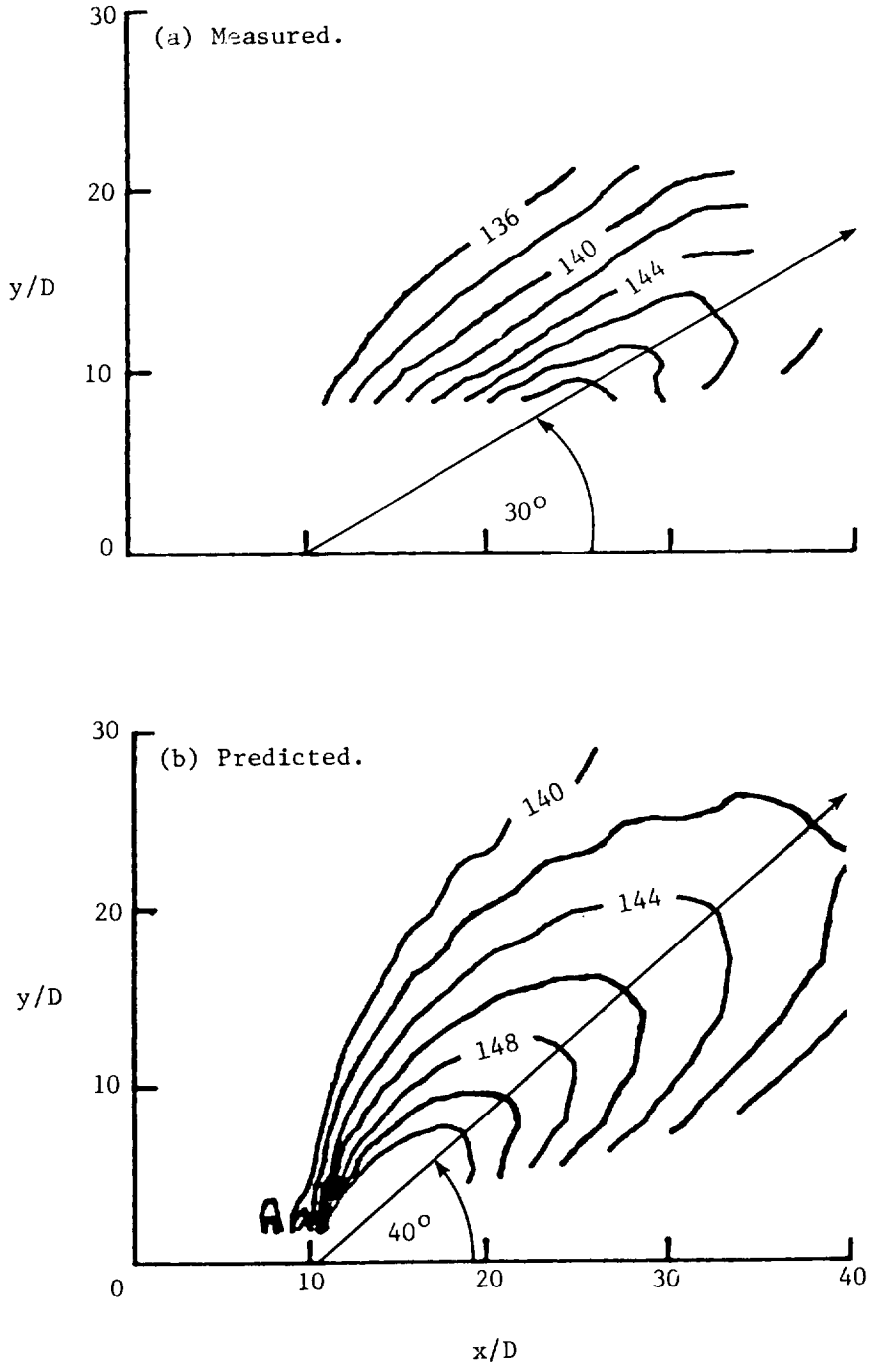

Figure 20.- Near-field sound pressure level contours for Re = 7.9×10^3, Mach 2.1 jet.

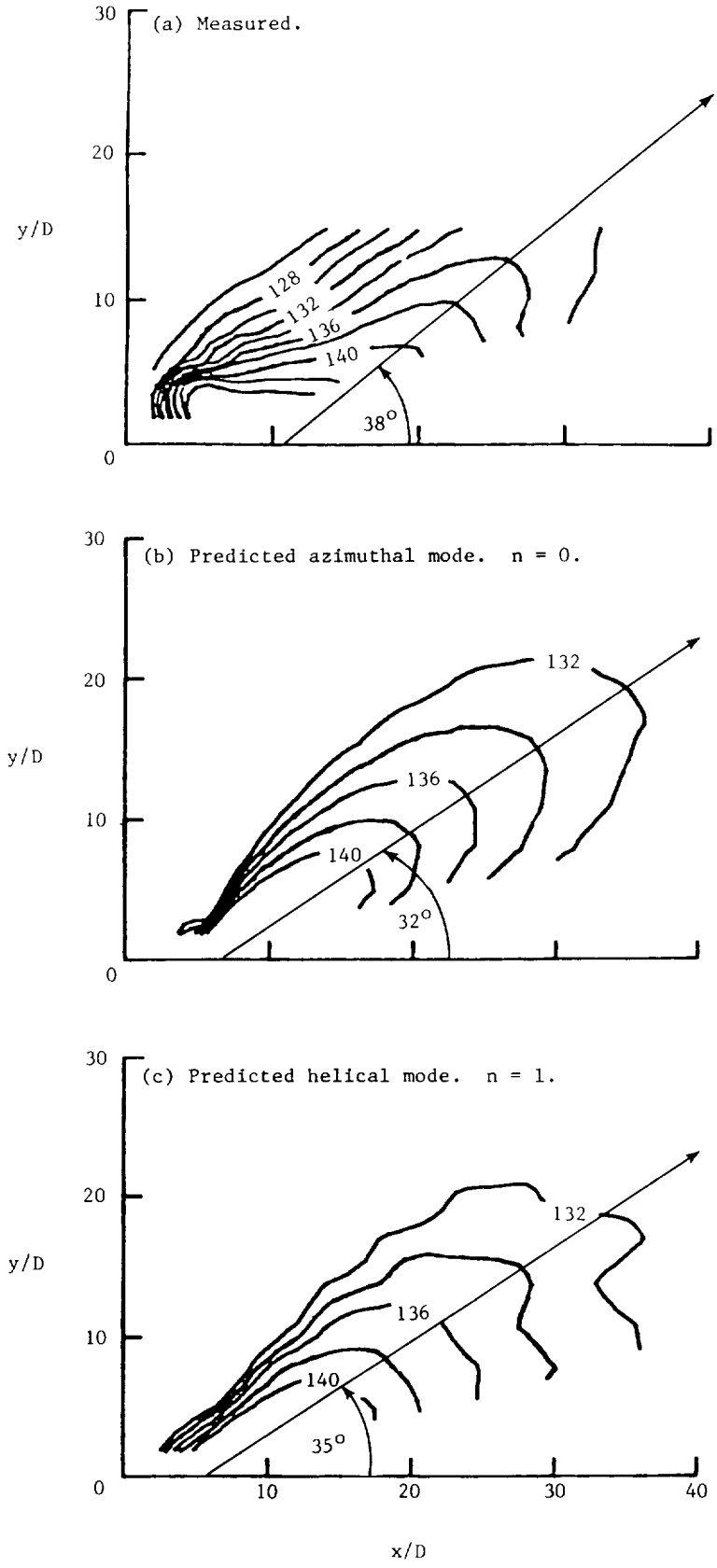

Figure 21.- Near-field sound pressure level contours for Re = 7.0×10^4, Mach 2.1 jet at St = 0.19.

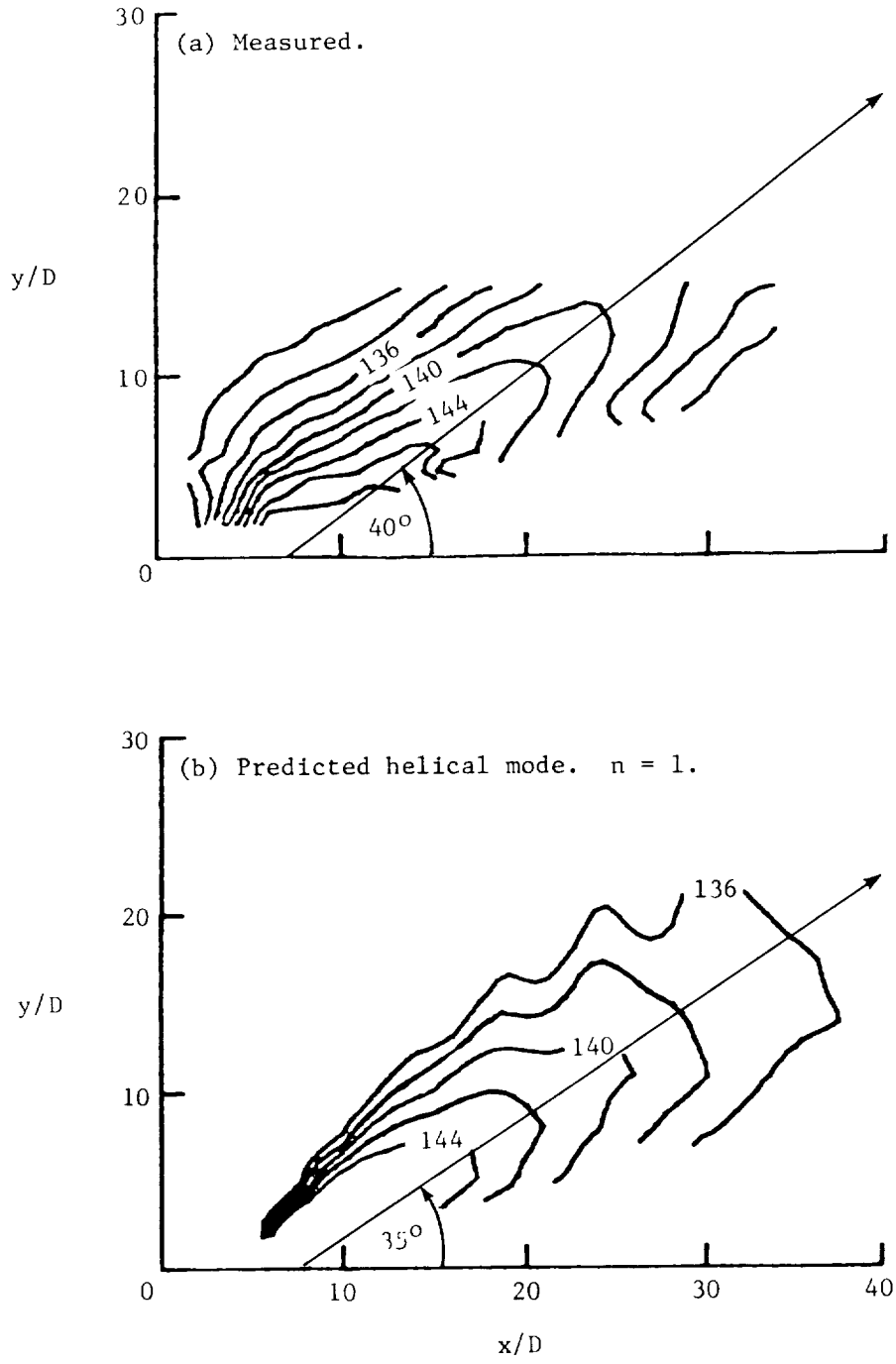

Figure 22.- Near-field sound pressure level contours for $Re = 7.0 \times 10^4$, Mach 2.1 jet at St = 0.38.

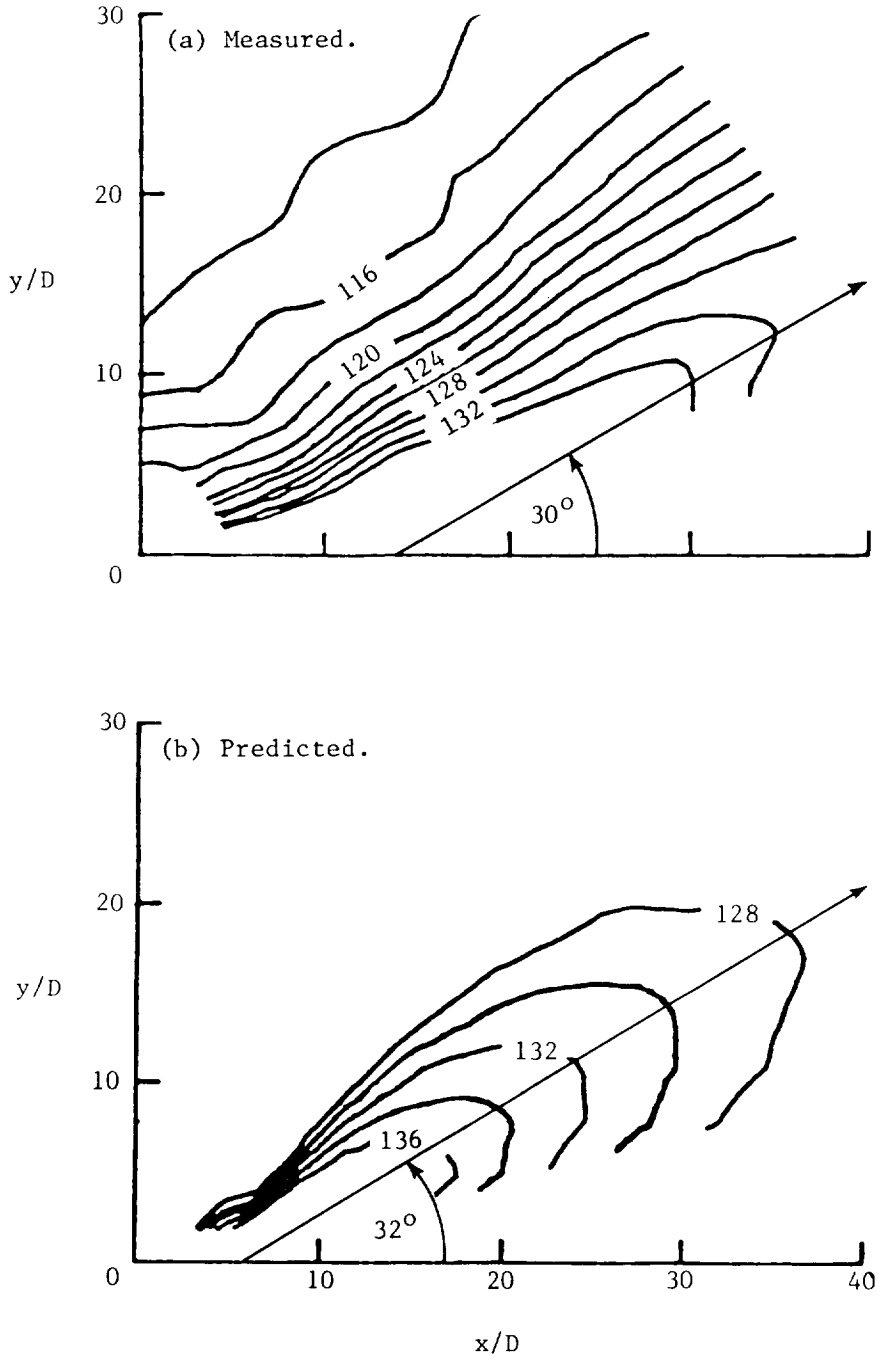

Figure 23.- Near-field sound pressure level contours for Re = 5.2 x 10^6, Mach 2.0 jet at St = 0.2 (1/3-octave band).

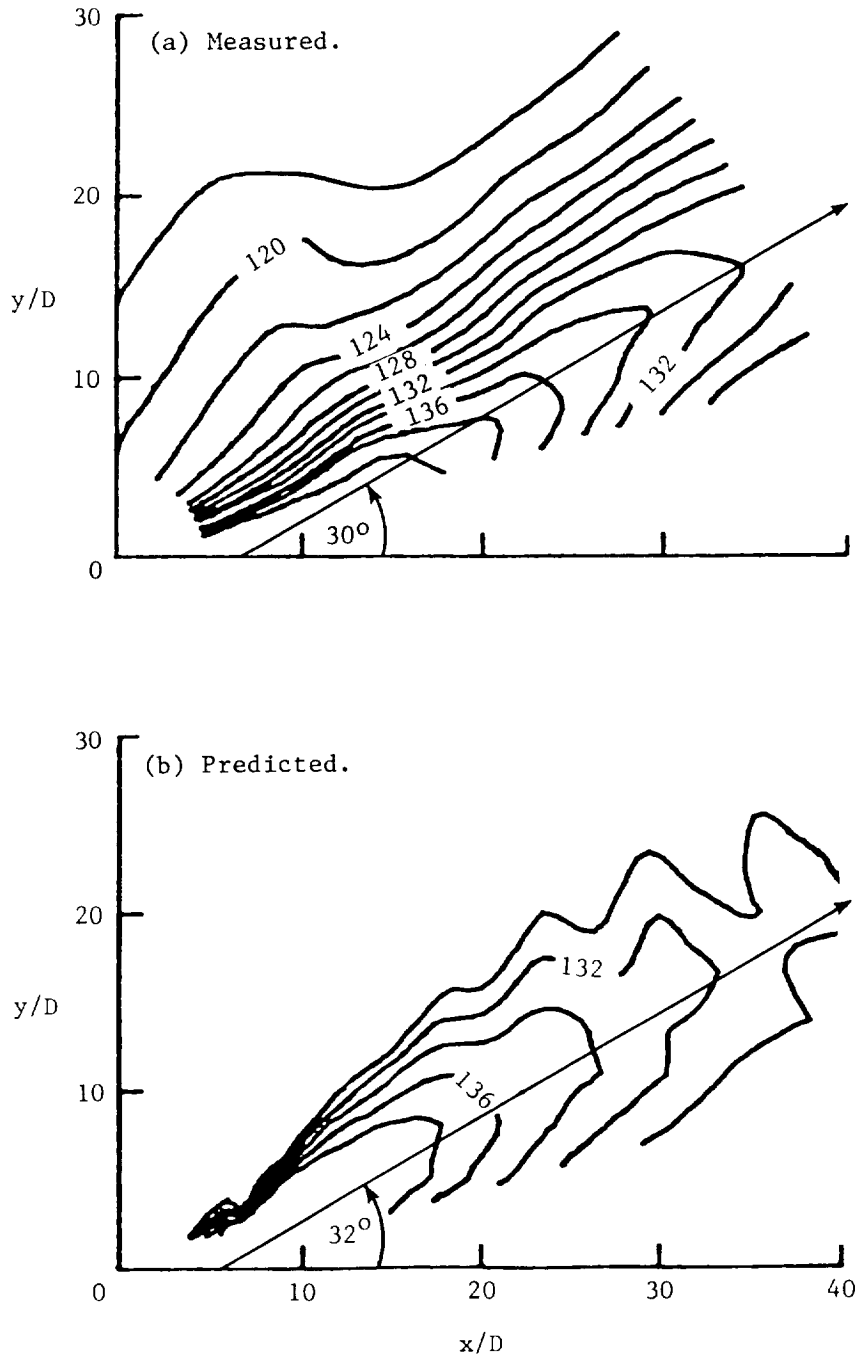

Figure 24.- Near-field sound pressure level contours for Re = 5.2×10^6, Mach 2.0 jet as St = 0.4 (1/3-octave band).

1. Report No.	2. Government Accession No.	3. Recipient's Catalog No.
NASA TP-2072		

4. Title and Subtitle	5. Report Date
SUPERSONIC JET NOISE GENERATED BY LARGE-SCALE INSTABILITIES	September 1982
	6. Performing Organization Code: 505-32-03-05

7. Author(s)	8. Performing Organization Report No.
John M. Seiner, Dennis K. McLaughlin, and C. H. Liu	L-15307
	10. Work Unit No.

9. Performing Organization Name and Address	11. Contract or Grant No.
NASA Langley Research Center Hampton, VA 23665	
	13. Type of Report and Period Covered: Technical Paper

12. Sponsoring Agency Name and Address	14. Sponsoring Agency Code
National Aeronautics and Space Administration Washington, DC 20546	

15. Supplementary Notes

16. Abstract

This paper examines the role of large-scale wavelike structures as the major mechanism for supersonic jet noise emission. With the use of previously published aerodynamic and acoustic data for low Reynolds number, supersonic jets at and below 7.0×10^4, comparisons are made with new flow fluctuation and acoustic measurements in high Reynolds number, supersonic jets. These comparisons show that a similar physical mechanism governs the generation of sound emitted in the principal noise direction. These experimental data are further compared with a linear instability theory whose prediction for the axial location of peak wave amplitude agrees satisfactorily with measured phased-averaged flow fluctuation data in the low Reynolds number jets. The agreement between theory and experiment in the high Reynolds number flow differs as to the axial location for peak flow fluctuations and predicts an apparent origin for sound emission far upstream of the measured acoustic data.

17. Key Words (Suggested by Author(s))	18. Distribution Statement
Supersonic Jet noise Coherent structure	Unclassified - Unlimited Subject Category 71

19. Security Classif. (of this report)	20. Security Classif. (of this page)	21. No. of Pages	22. Price
Unclassified	Unclassified	43	A03

For sale by the National Technical Information Service, Springfield, Virginia 22161

NASA-Langley, 1982